**Atmospheric
Chemistry
and Physics
Discussions**

Submicron particles influenced by mixed biogenic and anthropogenic emissions: high-resolution aerosol mass spectrometry results from the Carbonaceous Aerosols and Radiative Effects Study (CARES)

A. Setyan[1], Q. Zhang[1], M. Merkel[2], W. B. Knighton[3], Y. Sun[4], C. Song[5], J. E. Shilling[5], T. B. Onasch[6], S. C. Herndon[6], D. R. Worsnop[6], J. D. Fast[5], R. A. Zaveri[5], L. K. Berg[5], A. Wiedensohler[2], B. A. Flowers[7], M. K. Dubey[7], and R. Subramanian[8]

[1]Department of Environmental Toxicology, University of California, Davis, CA 95616, USA
[2]Leibniz Institute for Tropospheric Research, 04318 Leipzig, Germany
[3]Montana State University, Bozeman, MT 59717, USA
[4]Institute of Atmospheric Physics, Chinese Academy of Science, Beijing, China

Discussion Paper | Discussion Paper | Discussion Paper | Discussion Paper

ACPD

12, 5601–5658, 2012

Submicron particles influenced by emissions

A. Setyan et al.

Title Page

Abstract | Introduction

Conclusions | References

Tables | Figures

◄ | ►

◄ | ►

Back | Close

Full Screen / Esc

Printer-friendly Version

Interactive Discussion

[5]Pacific Northwest National Laboratory, Richland, WA 99352, USA
[6]Aerodyne Research Inc., Billerica, MA 01821, USA
[7]Los Alamos National Laboratory, Los Alamos, NM 87545, USA
[8]Droplet Measurement Technologies, Boulder, CO 80301, USA

Correspondence to: Q. Zhang (dkwzhang@ucdavis.edu)

Title Page

Abstract | Introduction

Conclusions | References

Tables | Figures

|◄ | ►|

◄ | ►

Back | Close

Full Screen / Esc

Printer-friendly Version

Interactive Discussion

Full Screen / Esc

Printer-friendly Version

Interactive Discussion

Abstract

The Carbonaceous Aerosols and Radiative Effects Study (CARES) took place in the Sacramento Valley of California in summer 2010. We present results obtained at Cool, CA, the T1 site of the project (~ 40 km downwind of urban emissions from Sacramento), where we deployed an Aerodyne high resolution time-of-flight aerosol mass spectrometer (HR-ToF-AMS) in parallel with complementary instrumentation to characterize the sources and processes of submicron particles (PM_1). Cool is located at the foothill of the Sierra Nevada Mountains, where intense biogenic emissions are periodically mixed with urban outflow transported by daytime southwesterly winds from the Sacramento metropolitan area. The particle mass loading was low ($3.0\,\mu g\,m^{-3}$ on average) and dominated by organics (80 % of the PM_1 mass) followed by sulfate (9.9 %). Organics and sulfate appeared to be externally mixed, as suggested by their different time series ($r^2 = 0.13$) and size distributions. Sulfate showed a bimodal distribution with a droplet mode peaking at ~ 400 nm in vacuum aerodynamic diameter (D_{va}), and a condensation mode at ~ 150 nm, while organics generally displayed a broad distribution in 60–600 nm (D_{va}). New particle formation and growth events were observed almost every day, emphasizing the roles of organics and sulfate in new particle growth, especially that of organics. The organic aerosol (OA) had a nominal formula of $C_1H_{1.38}N_{0.004}O_{0.44}$, thus an average organic mass-to-carbon (OM/OC) ratio of 1.70. Two different oxygenated OA (OOA, 90 % of total OA mass) and a hydrocarbon-like OA (HOA, 10 %) were identified by Positive matrix factorization (PMF) of the high-resolution mass spectra. The more oxidized MO-OOA (O/C = 0.54) corresponded to secondary OA (SOA) primarily influenced by biogenic emissions, while the less oxidized LO-OOA (O/C = 0.42) corresponded to SOA associated with urban transport. The HOA factor corresponded to primary emissions mainly due to local traffic. Twenty three periods of urban plumes from T0 (Sacramento) to T1 (Cool) were identified using the Weather Research and Forecasting model coupled with Chemistry (WRF-Chem). The average PM_1 mass loading was much higher in urban plumes

Submicron particles influenced by emissions

A. Setyan et al.

($3.9\,\mu\mathrm{g\,m^{-3}}$) than in air masses dominated by biogenic SOA ($1.8\,\mu\mathrm{g\,m^{-3}}$). The change in OA mass relative to CO ($\Delta\mathrm{OA}/\Delta\mathrm{CO}$) varied in the range of $5\text{–}196\,\mu\mathrm{g\,m^{-3}\,ppm^{-1}}$, reflecting large variability in SOA production. The highest $\Delta\mathrm{OA}/\Delta\mathrm{CO}$ were reached when urban plumes arrived at Cool in the presence of a high concentration of biogenic volatile organic compounds (BVOCs = isoprene + monoterpenes + 2-methyl-3-buten-2-ol [MBO] + methyl chavicol). This ratio, which was $77\,\mu\mathrm{g\,m^{-3}\,ppm^{-1}}$ on average when BVOCs > 2 ppb, is much higher than when urban plumes arrived in a low biogenic VOCs environment ($28\,\mu\mathrm{g\,m^{-3}\,ppm^{-1}}$ when BVOCs < 0.7 ppb) or during other periods dominated by biogenic SOA ($40\,\mu\mathrm{g\,m^{-3}\,ppm^{-1}}$). The results from this study demonstrate that SOA formation is enhanced when anthropogenic emissions interact with biogenic precursors.

1 Introduction

Atmospheric aerosols significantly affect the Earth's climate (IPCC, 2007), human health (Pope et al., 2009), ecological balance (Mahowald, 2011), and visibility (Watson, 2002). Aerosols are constituted of a wide range of chemical compounds, such as sulfate, nitrate, ammonium, sea salt, crustal species from soil dust, water, and carbonaceous materials (Seinfeld and Pandis, 2006). However, the analysis of many datasets from around the world showed that organic species generally represent the dominant fraction and account for 20–90 % of the mass in submicron particles ($\mathrm{PM_1}$) (Zhang et al., 2007a). Organic aerosols (OA) are classified into primary (POA) or secondary (SOA). POA refers to aerosols directly emitted by a source, such as fossil fuel combustion, biomass burning or food cooking, while SOA are generated by reactions of gaseous precursors. In addition to the formation mechanisms, organic aerosols are also classified depending on their sources, e.g., biogenic or anthropogenic.

Models have been developed to improve understanding of aerosol processes and properties, and to evaluate their effects on climate. Even if some uncertainties still remain, the processes controlling the formation and evolution of inorganic compounds

are now well understood (Zaveri et al., 2008). On the other hand, SOA formation is controlled by very complex processes, which include photo-oxidation of volatile organic compounds (VOCs), nucleation or gas-to-particle partitioning of low volatile compounds onto preexisting particles, and aqueous-phase and heterogeneous processes
(Kanakidou et al., 2005; Hallquist et al., 2009; Ervens et al., 2011). Current box and 3-D models have difficulty predicting accurately SOA concentrations and/or properties (e.g., Volkamer et al., 2006; Dzepina et al., 2009). Recent studies suggest that anthropogenic and biogenic emissions may interact and increase SOA formation (Kanakidou et al., 2000; Weber et al., 2007; Goldstein et al., 2009 Hoyle et al., 2011; Worton et al.,
2011). Thus, field campaigns have been undertaken in locations subjected to both urban and natural influences to study the enhancement effects of SOA production in mixed biogenic and anthropogenic emissions. These studies are important for identifying missing SOA sources in current models and closing the gaps between simulated and measured SOA concentrations and properties (Zaveri et al., 2012).

The Sacramento Valley, which corresponds to the northern part of the California Central Valley, is a place of choice to study processes of organic species from biogenic and anthropogenic sources. The valley forms a northwest-southeast axis and its shape is defined by mountains on the west (various Coast Ranges), north (Siskiyou Mountains) and east (Sierra Nevada Mountains). A mid-size metropolitan area (Sacramento and its suburbs) lies on the south edge of the valley, while the rest of the valley is heavily forested and contains large agricultural regions. The Sacramento Valley has faced air pollution problems such as high ozone concentrations promoted by meteorological conditions (strong sunlight and high temperatures) coupled with high VOCs and NO_x emissions (Murphy et al., 2007). In summer, the region is subjected to constant winds, which bring air masses from the Pacific Ocean to the Sacramento metropolitan area, and push northeast to the Sierra Nevada Mountains, bringing urban outflow from Sacramento to the foothills (Dillon et al., 2002). Recent studies performed at the University of California-Blodgett Forest Research Station (UC-BFRS; Goldstein et al., 2000), which is located 75 km downwind from Sacramento and surrounded by a pon-

derosa pine plantation, pointed out that large amounts of reactive VOCs are emitted by the surrounding forests (e.g., Bouvier-Brown et al., 2009) and that SOA formation in this region is mainly driven by oxidation of monoterpenes and isoprene (Cahill et al., 2006; Worton et al., 2011) mediated primarily by ozone (Holzinger et al., 2005). New

5 particle formation and growth events (Lunden et al., 2006; Creamean et al., 2011) have been frequently observed as well, indicating the importance of secondary aerosol formation processes in the region. Several studies also focused on chemical processes occurring in urban plumes brought from Sacramento (Dillon et al., 2002; Spaulding et al., 2003), but anthropogenic influences were found to be small at the UC-BFRS,

10 probably because the site is too far from significant urban emission sources.

The Carbonaceous Aerosols and Radiative Effects Study (CARES), which was sponsored by the US Department of Energy (DOE), took place in California in summer 2010. The aim of this field campaign was to better understand the evolution and ageing of carbonaceous aerosols in a region influenced by mixed anthropogenic and biogenic

15 precursors, and to integrate this knowledge into models used for simulating their direct and indirect radiative effects on climate (Fast et al., 2012; Zaveri et al., 2012). Measurements were conducted at two ground-based sites: one within the Sacramento urban area (denoted T0 to represent the urban emission origin of the project) and one at Cool, CA (denoted T1 to represent a rural receptor site located $\sim 40\,\text{km}$ northeast

20 of, i.e., downwind from, T0). In coordination with the two ground-based operations, two aircrafts conducted regular flights through and around the Sacramento plumes during CARES. Zaveri et al. (2012) provide a complete overview of the CARES field campaign, including a description of the experimental design and key observations from the two ground-based sites and aircraft platforms.

25 In this paper, we present results obtained at the T1 site of CARES, where we deployed an Aerodyne HR-ToF-AMS in parallel with a scanning mobility particle sizer (SMPS) to characterize the concentration, chemical composition, size distribution, and temporal variation of submicron particles (PM$_1$). We performed positive matrix factorization (PMF) of the high resolution mass spectra to identify distinct OA factors and

Submicron particles influenced by emissions

A. Setyan et al.

determine their concentrations and mass spectra. These results were combined with collocated measurements of other aerosol properties, trace gases, and meteorological conditions to elucidate the sources of and processes controlling PM_1 at T1. Finally, periods of urban plumes from Sacramento and other air masses dominated by biogenic emissions were determined by the WRF-Chem model (Fast et al., 2012). Aerosols during different periods are compared to study the influence of anthropogenic emissions on the formation of biogenic SOAs.

2   Methods

2.1   Sampling site, instrumentation, meteorological conditions, and time

The CARES field campaign took place in the Sacramento Valley between 2 June and 28 June 2010. A map of the Sacramento Valley with the location of the two ground-based sites is given in Fig. 1a. Measurements reported in this paper were performed at Cool (T1 site; 38°53′ N, 121°00′ W) in a maintenance parking lot on the campus of the Northside School. Cool is a small town (2500 inhabitants) located at the foothills of the Sierra Nevada Mountains at an elevation of 450 m a.s.l. The sampling site is surrounded by forests, and located ∼200 m from the California State Route 49. During summer, Cool is influenced by highly consistent winds bringing urban outflow from Sacramento during the afternoon (Dillon et al., 2002). A complete description of the meteorological conditions during the CARES is given by Fast et al. (2012). In summary, the meteorological conditions were spring like, with high temperatures (on average 27 °C during the day and 14 °C in the night; Fig. S2a) and a consistent but weak southwesterly wind during the day (Fig. 1b). The weather was sunny during the entire campaign, except for two cloudy periods on 4 and 24 June 2010. In addition, during the present study, transport of pollutants from Sacramento over the Sierra Nevada foothills occurred almost every afternoon except for three periods (Fast et al., 2012).

Various instruments installed in two adjacent trailers were used in parallel to mea-

Submicron particles influenced by emissions

A. Setyan et al.

Title Page

Abstract	Introduction
Conclusions	References
Tables	Figures

◀◀   ▶▶

◀   ▶

Back   Close

Full Screen / Esc

Printer-friendly Version

Interactive Discussion

sure the concentration, chemical composition, size distribution, mixing state, radiative and optical properties, and cloud condensation nuclei (CCN) activities of particles, as well as trace gas concentrations and meteorological conditions (Zaveri et al., 2012). A schematic drawing of the instrumental setup for PM_1 is given in Fig. 1c. Particles were sampled through a common inlet equipped with a PM_1 impactor (Brechtel Manufacturing Inc., Hayward, CA; model 8003) at a total flow rate of $\sim 15 \, l \, min^{-1}$. The air flow was sampled by a particle into liquid sampler (PILS), a CCN counter, and a temperature-controlled thermodenuder (TD). The sampling line downstream of the TD was split again in three parts to connect to an AMS, an SMPS, and a second CCN counter. A Nafion dryer was included in the system to dry particles analyzed by the AMS and SMPS. Additional instruments measuring aerosol size and composition, including a single particle soot photometer (SP2) and a particle analysis by laser mass spectrometry (PALMS) system, aerosol optical properties, and trace gases (e.g., VOCs by proton transfer reaction mass spectrometer (PTR-MS), CO, CO_2, CH_4, H_2O, and ozone) were also deployed at T1, but shared other common inlets.

All dates and times reported in this paper are in Pacific Daylight Time (PDT), which was the local time during this study. PDT corresponds to the Coordinated Universal Time (UTC) minus 7 h and the Pacific Standard Time (PST) plus 1 h.

2.2 High resolution aerosol mass spectrometer

2.2.1 Operation

An HR-AMS (DeCarlo et al., 2006; Canagaratna et al., 2007) was used to measure the size-resolved chemical composition of non-refractory submicron aerosols (NR-PM_1) in the size range 35–1000 nm in D_{va}. The D_{va} measured by the AMS corresponds to the product of the geometric diameter (or Stokes diameter, D_s) and the particle density (1.4 g cm^{-3} in average during this study, see Sect. 3.1.1) (DeCarlo et al., 2004).

In brief, particles are sampled into a high vacuum system ($\sim 10^{-5}$ Pa) through a 100 µm critical orifice and an aerodynamic lens installed at the inlet of the instru-

ment. The narrow particle beam formed after the passage through the lens crosses a particle time-of-flight (PToF) region, where the measurement of the velocity allows the determination of the particle diameter in D_{va}. Particles are then transmitted into a detection chamber, where non-refractory components (organics, sulfate, nitrate, ammonium, and chloride) are vaporized upon impact on a metallic surface heated up to $\sim 600\,°C$, and ionized by electron impact (70 eV). The chemical composition of the particles is finally determined by a high resolution time-of-flight mass spectrometer. The mass particles is finally determined by a high resolution time-of-flight mass spectrometer operated alternatively in two modes – "V" and "W". The V-mode is more sensitive than the W-mode, while the mass resolution of the W-mode is much higher (~ 5000 vs. ~ 2500 for V-mode).

The data acquisition was performed using the ToF-AMS Data Acquisition software v3.0.29, available online at http://cires.colorado.edu/jimenez-group/wiki/index.php/ToF-AMS_DAQ. Between 2 June and 17 June 2010, the HR-AMS was operated under the V- and W-modes alternatively every 2.5 min. From 17 June till the end of the field campaign (28 June), a temperature-stepping thermodenuder was operated upstream of the AMS, SMPS and CCN #2 (Fig. 1c). During this period, a valve switched automatically every 5 min to alternate the air flow sampled by the instruments between a bypass (ambient temperature) and the heated section of the thermodenuder. During the bypass period, the AMS was still operated under the V- and W-modes (2.5 min each), while during the thermodenuder period, two runs under the V-mode were acquired (also 2.5 min each). PToF data was systematically acquired in the V-mode, but not in the W-mode, due to low signal/noise ratio.

The ionization efficiency (IE) of the HR-AMS was calibrated at the beginning, in the middle and at the end of the field campaign, following a standard protocol previously published (Jayne et al., 2000). The IE/air beam ratio varied less than 3 % between the beginning and the end of the campaign, indicating that the instrument remained remarkably stable during the four weeks of the study. For the relative ionization efficiencies (RIEs) of the main chemical species, we used values previously published for

organics (1.4), nitrate (1.1) and chloride (1.3) (Alfarra et al., 2004). The RIE of ammonium was determined at 4.0 following the NH_4NO_3 analysis during the IE calibrations, and that of sulfate was determined at 1.4 following the analysis of pure $(NH_4)_2SO_4$. The particle sizing was calibrated at the same time as the IE calibration using polystyrene latex spheres of known sizes (Duke Scientific, Palo Alto, California). A total 13 different sizes in the range of 22–700 nm were used. Finally, two particulate-free periods were recorded before and after the campaign using a HEPA filter (Pall Corp., model 12144), for subsequent adjustment of the fragmentation table and determination of the detection limits of individual species (see below).

2.2.2 Data analysis

The data analysis was performed using SQUIRREL v1.51 and PIKA v1.10, the standard ToF-AMS analysis toolkits used on Igor Pro 6.2.2.2 (WaveMetrics Inc., OR) and available online at http://cires.colorado.edu/jimenez-group/ToFAMSResources/ ToFSoftware/index.html. The V-mode and PToF data were processed with SQUIRREL to determine the mass concentrations and size distributions of NR-PM$_1$ species. The ammonium concentrations, however, were determined from PIKA analysis of the V-mode data since those from the SQUIRREL analysis are too noisy. Figure S1 in the Supplement shows the comparison of the ammonium time series between SQUIRREL and PIKA. The W-mode data was processed with PIKA to obtain high resolution mass spectra and the elemental composition of organic species.

In order to apportion correctly the ToF-MS signal into the different chemical species, the fragmentation tables of SQUIRREL and PIKA were adjusted according to the method presented by Allan et al. (2004). The detection limit of individual species was determined as three times the standard deviation of the corresponding signal in particle-free air (Zhang et al., 2005b). The 2.5-min detection limits are 0.075 (organics), 0.011 (sulfate), 0.018 (nitrate), 0.010 (ammonium), and 0.017 µg m^{-3} (chloride).

A collection efficiency (CE) was introduced to take into account of incomplete detection of aerosols, due to e.g., particle bounce at the vaporizer (Matthew et al., 2008). In

most of the previous field campaigns, a constant CE of 0.5 for all the species has been found to be consistent with results obtained with collocated instruments. However, CE may increase depending on the chemical composition (e.g., mass fraction of NH_4NO_3), acidity, water content and the phase of the particle (Kleinman et al., 2007; Middlebrook et al., 2012). We use a constant CE of 0.5 for all the species in this study, because 1) particles were dominated by organics during the entire campaign (see Sect. 3.1.1), 2) they appeared to be fully neutralized (Fig. 4), and 3) the air flow was dried (RH < 30 %) prior to the AMS analysis. This choice has been validated by the inter-comparison between AMS + BC mass and SMPS volume (Figs. 2a and 3).

PMF analysis was performed on the high resolution mass spectra of organic species to determine the mass spectra of distinct organic factors and their time-dependent concentrations. This technique was described by Paatero and Tapper (1994), while its application to AMS datasets was discussed by Ulbrich et al. (2009) and reviewed by Zhang et al. (2011). Data and error matrices were first generated in PIKA. The error matrix was then further adjusted to take into account of the counting error of ions by the detector (Ulbrich et al., 2009). Ions with a signal-to-noise ratio (S/N) < 0.2 were removed from the data and error matrices, while ions whose S/N were between 0.2 and 2 were down-weighed by a factor of 3. Four organic ions scaled to the CO_2^+ signal (O^+, HO^+, H_2O^+, and CO^+) were removed from the data and error matrices prior to the PMF analysis. They were reintroduced in the mass spectra after the PMF analysis. PMF analysis was performed using the PMF Evaluation Tool Software v2.03A described in Ulbrich et al. (2009), available online at http://cires.colorado.edu/jimenez-group/wiki/index.php/PMF-AMS_Analysis_Guide. The PMF has been tested from 1 to 10 factors and for FPEAK values between −1 and +1 (step: 0.1). The best solution has been chosen based on the evaluation procedures given in Table 1 of Zhang et al. (2011). A summary of the evaluation of the PMF results is given in Figs. S3 and S4.

Submicron particles influenced by emissions

A. Setyan et al.

2.3 Collocated measurements

An SMPS was used to measure the particle number size distribution in the range from 8 to 858 nm in D_m. The SMPS used during this study followed a recommended standard design of the European supersites (Wiedensohler et al., 2010) for atmospheric measurements and was manufactured by the WMO-GAW World Calibration Center for Aerosol Physics (WCCAP) hosted at the Leibnitz Leipzig Institute for Tropospheric Research. The instrument consists of a neutralizer (Po^{210}), a Hauke-type differential mobility analyzer (DMA; design described by Winklmayr et al., 1991) and a condensation particle counter (CPC; TSI Inc., MN; model 3772). The SMPS alternated between two modes – the "upscan" mode (from 8 to 858 nm) and the "downscan" mode (from 858 to 8 nm) – every 2.5 min. The data was recorded every 5 min, corresponding to the average of the "upscan" and "downscan" modes alternatively. The aerosol sampling flow was set at 1 l min^{-1}, and was obtained by using a vacuum pump (GAST Manufacturing Inc., MI; model DOA-P704-AA) connected to the outlet of the CPC. The sheath flow was set at 5 l min^{-1}. The data acquisition software applied correction for the DMA transfer function (Birmili et al., 1997) and the bipolar charge distribution (Wiedensohler, 1988) to enable a mathematical correction for particles whose mobility was affected due to multiple charges. The corrections for the CPC efficiency and the internal diffusion losses were applied after the data inversion. The diffusion losses were calculated following the methods of the "equivalent length" (Wiedensohler et al., 2010).

A PTR-MS (de Gouw and Warneke, 2007) was used for online monitoring of VOCs. Briefly, H_3O^+ ions are produced in a hollow-cathode discharge in water vapor, and are injected into the drift tube reaction region where they interact with the ambient sample. These reagent ions are pulled through the ambient sample at reduced pressure ($\sim$ 2 mbar) under the influence of an applied electric field where they will transfer a proton to any component having a proton affinity greater than that of water. A fraction of the reagent ions and product ions formed are sampled through a small aperture at the end of drift tube and mass analyzed using a quadrupole mass spectrometer operated in the

ion counting mode. For the present study, the ratio between the electric field strength and the buffer gas density (E/N ratio) was 133–136 Td between 2 and 4 June 2010, and 139 Td from 4 June until the end of the campaign.

The black carbon (BC) concentration was measured with a SP2 (Droplet Measurement Technologies) (Subramanian et al., 2010). Briefly, particles containing BC absorb energy from an Nd : YAG laser and are heated to the point of incandescence. The incandescence is measured and correlated to the particle's BC mass using BC proxies; the results presented here are based on an Acheson Aquadag[®]-based calibration. In addition, the concentration of CO (Teledyne, model M300EU), CO_2 and CH_4 (Picarro, model 1301G-M), and O_3 (Thermo Scientific, model 49i) were measured.

2.4 WRF-Chem and air mass classification

The WRF-Chem model was used to determine periods of urban plumes from T0 to T1. Details on the operation of the model are given by Fast et al. (2012). Briefly, the model was run to forecast the spatial and temporal variations of CO emitted by 20 anthropogenic sources. Spatial distribution of these sources includes regions from the San Francisco Bay Area up to the Sierra Nevada foothills, and from the Sacramento Valley to Southern California. Urban plumes were determined as periods during which CO emitted in the Sacramento region contributed to more than 30 % of the total anthropogenic CO at T1. In total, 23 periods of urban plumes were identified during this study, brought by southwesterly wind favorable to the transport of pollutants from Sacramento to Cool. Eight of these periods were characterized by an air mass transported directly from Sacramento to Cool following a straight path, while during twelve other periods the air mass was transported either to the north or to the south of T1 before being redirected to T1. The remaining three periods consisted of recirculation of aged plumes over the foothills. A second modeling system, the North American Mesoscale (NAM), identified three periods (10–13 June, 16–17 June, 20–21 June) during which the meteorology was characterized by the passage of mid-tropospheric troughs over California,

Title Page

Abstract | Introduction

Conclusions | References

Tables | Figures

◀ | ▶

◀ | ▶

Back | Close

Full Screen / Esc

Printer-friendly Version

Interactive Discussion

resulting in a shift of the wind direction from the southwest to the northwest. Therefore, during these eight days, urban plumes were transported to the southeast of Sacramento while the T1 site was influenced by clean air masses coming from the northwest, reducing considerably the concentration of pollutants at T1. Finally, another air mass was brought to the T1 site during the night, when the decrease of the temperature reversed the wind direction and favored downslope flows from the Western Sierra Nevada back to the Sacramento Valley. These different periods determined by model predictions and given by Fast et al. (2012) were slightly refined in the present study using wind data recorded at T1 and the results of the PMF analysis, which identified among others an oxygenated organic aerosol (OOA) component resulting from urban transport (see Sect. 3.2). The periods are marked on Fig. 2.

3   Results and discussions

3.1   Overview of submicron aerosol characteristics

3.1.1   Concentrations and chemical composition of submicron aerosols

The particle mass concentration was low at T1, varied between 0.4 and 13.8 $\mu g\,m^{-3}$ and the average over the entire study was 3.0 $\mu g\,m^{-3}$ (Table 1). The chemical composition was dominated by organics, which on average accounted for 80 % of the total particle mass, with smaller but significant contributions from sulfate (9.9 %), ammonium (4.5 %), nitrate (3.6 %), and BC (1.6 %). The chloride concentration was below detection limit during more than 90 % of the study. Similar PM_1 composition and loading was determined during the BEARPEX 2007 field campaign at the Blodgett Forest, which is located 35 km to the northeast (i.e., downwind) of the site of the present study (Farmer et al., 2011; Worton et al., 2011). While forest fires may occur in the region during summer (Worton et al., 2011) we have found no indication of wildfires during the present study based on the time series of Org 60 (mainly the $C_2H_4O_2^+$ ion) and Org

73 ($C_3H_5O_2^+$), two key tracers of biomass burning in AMS mass spectra (Alfarra et al., 2007). In addition, the potassium signal recorded by the AMS as well as the gas phase acetonitrile measured using PTR/MS (Fig. S2f) remained low during the entire study, further indicating the lack of biomass burning influence at T1.

The AMS and SMPS agreed very well throughout this study (Fig. 3). The slope of the scatter plot (1.42) corresponds to the average particle density throughout the study, and is consistent with results obtained with a single particle laser ablation time-of-flight mass spectrometer at the T0 site (Vaden et al., 2011). We estimated the density of organics at $1.33\,\mathrm{g\,cm^{-3}}$ by subtracting the contribution of the other chemical species, using the known densities for ammonium sulfate (1.78), ammonium nitrate (1.72) and ammonium chloride (1.53), and a density of 1.8 for BC based on values recommended by Bond and Bergstrom (2006). We also predicted the density of organics using the average O/C and H/C ratios based on the formula reported in Kuwata et al. (2012):

$$\rho_{\mathrm{org}} = [12 + 1 \cdot (\mathrm{H/C}) + 16 \cdot (\mathrm{O/C})]/[7 + 5 \cdot (\mathrm{H/C}) + 4.15 \cdot (\mathrm{O/C})] \tag{1}$$

in which ρ_{org} is the density of organics ($\mathrm{g\,cm^{-3}}$), H/C and O/C are the average values (1.38 and 0.44, respectively) throughout the study (see Sect. 3.1.4). The density of organics predicted with this method is $1.30\,\mathrm{g\,cm^{-3}}$, very close to the value of 1.33 obtained based on particulate mass vs. volume comparison.

Submicron particles appeared to be bulk neutralized at T1, as shown in the scatter plot of measured NH_4^+ concentration vs. that predicted assuming anions being fully neutralized by NH_4^+ (Fig. 4):

$$NH_4^+ \text{ predicted} = (2 \cdot 18/96 \cdot SO_4^{2-}) + (18/62 \cdot NO_3^-) + (18/35.5 \cdot Cl^-) \tag{2}$$

where NH_4^+, SO_4^{2-}, NO_3^-, and Cl^- denote the mass concentrations (in $\mathrm{\mu g\,m^{-3}}$) of the species and the denominators correspond to their molecular weights. This equation and its application to inferring particle acidity have been presented and discussed in detail by Zhang et al. (2007b). The slope is very close to 1 (0.97; Fig. 4), suggesting that sulfate presents in the form of ammonium sulfate $(NH_4)_2SO_4$ at T1. Neutralized

particles were observed at the Blodgett Forest as well (Farmer et al., 2011). These results are consistent with the presence of large agricultural regions and thus abundant ammonia emissions in the Sacramento Valley (Clausnitzer and Singer, 1996).

Nitrate accounted for a minor fraction of the particle mass (3.6 %; average $= 0.11\,\mu g\,m^{-3}$) at T1. The signal of nitrate was dominated by two ions, NO^+ (m/z 30) and NO_2^+ (m/z 46), which taken together accounted for 94 % of the total signal of nitrate. In this study, we noticed a much higher slope of NO^+ vs. NO_2^+ in ambient particles than in pure NH_4NO_3 used for the IE calibrations (6.8 vs. 1.7), indicating that an important part of the nitrate signal is not due to ammonium nitrate but possibly correspond to organonitrates or metal nitrates (Farmer et al., 2010). The NO^+/NO_2^+ ratio can vary dramatically, depending on the nitrate compound. For example, Farmer et al. (2010) reports a NO^+/NO_2^+ ratio of 1.5 for NH_4NO_3 and an average of 3.5 for various organonitrate standards (min: 1.8, max: 4.5), while Rollins et al. (2010) measured a NO^+/NO_2^+ ratio in the range 0.99–5.3 for laboratory-generated organonitrates and mentioned that this ratio can increase up to 29 for sodium nitrate. Moreover, Shilling et al. (2012) found NO^+/NO_2^+ ratios up to 8.8 for organic nitrates generated from trimethylbenzene. In this study, the presence of organonitrates was supported by the fact that 16 ions from the $C_xH_yO_zN_p^+$ family were observed in high resolution mass spectra, since organonitrates are reported as a source for these fragments (Farmer et al., 2010; Rollins et al., 2010). Moreover, organics and nitrate were reasonably well correlated during this study ($r^2 = 0.54$; Fig. 6b), although the correlation between organics and sulfate was poor ($r^2 = 0.13$; Fig. 6a). This result also suggests that a significant fraction of the nitrate signal could correspond to organonitrates. However, metal nitrates (such as sodium nitrate or potassium nitrate) could have been present as well, given that the NO^+/NO_2^+ ratios observed for ambient aerosols were higher than most of the organonitrates previously measured (Farmer et al., 2010; Rollins et al., 2010; Shilling et al., 2012). Assuming NO_2^+ being completely generated by NH_4NO_3 and using the ratio of nitrate mass vs. NO_2^+ signal obtained for pure NH_4NO_3 ($= 2.8$), we estimated that 35 % of the total nitrate presented in the form of NH_4NO_3 at T1. An upper bound of $0.060\,\mu g\,m^{-3}$

Title Page

Abstract	Introduction
Conclusions	References
Tables	Figures

|◀| |▶||

|◀| |▶|

Back | Close

Full Screen / Esc

Printer-friendly Version

Interactive Discussion

of the nitrate signal could be contributed by organonitrates and metal nitrates, which represents around an average 12 % of the total mole-equivalent concentration of the anions (= $SO_4^{2-}/48 + NO_3^-/62 + Cl^-/35.5$), indicating that the associated bias in the determination of the particle acidity was likely within the measurement uncertainties of
5 ammonium (Fig. 4).

Organosulfates might be present as well, given that we detected 11 ions from the $C_xH_yS_nO_z^+$ (x ≥ 1, y ≥ 1, n ≥ 1, z ≥ 0) family. Three of them ($CH_2SO_2^+$, $CH_3SO_2^+$ and $CH_4SO_3^+$) were well separated from adjacent ions in high resolution mass spectra, and their relative intensities ($CH_2SO_2^+/CH_3SO_2^+=0.32$; $CH_4SO_3^+/CH_3SO_2^+=0.32$) were
10 close to those in the mass spectrum of pure methanesulfonic acid (MSA; Ge et al., 2012), indicating the presence of this compound in PM_1. However, the total concentration of ions from the $C_xH_yS_nO_z^+$ family was only $2\,ng\,m^{-3}$, suggesting very limited contributions of organosulfates to the SOA and sulfate concentrations at T1. The close mole-equivalent balance between the anions (= sulfate + nitrate + chloride) and ammo-
15 nium further supports that the sulfate signal corresponded mainly to $(NH_4)_2SO_4$.

3.1.2 Size distribution of submicron aerosols

The average size distribution of total PM_1 mass showed a very broad mode extended from 60 to 600 nm in D_{va} (Fig. 5a). While submicrometer particles were dominated by organics in the entire size range, larger particles (> 300 nm) had a relatively larger con-
20 tribution (∼ 25 %) of ammonium sulfate compared to smaller particles (< 20 %) since these two species had very different size distributions (Fig. 5a). Sulfate showed a bimodal distribution with a prominent droplet mode at ∼ 400 nm (D_{va}) and a smaller condensation mode at ∼ 150 nm (D_{va}; Fig. 5b). In contrast, both organics and nitrate showed a broad unimodal distribution that peaks at 150–200 nm (D_{va}). Note that the
25 presence of nitrate at the same mode as organics was probably due to the fact that a significant fraction its signals was likely contributed by organonitrates, as discussed in Sect. 3.1.1.

The different size distributions of organics and sulfate and the poor correlation between their concentrations ($r^2 = 0.13$; Fig. 6a) suggest that these two species came from different sources and were likely externally mixed. For instance, the prominent droplet mode in the size distribution of sulfate indicates a significant influence of aqueous phase reactions on sulfate production. Indeed, the droplet mode particles are too large to be reached by gas to particle partitioning of low volatility compounds, while the growth of particles from the condensation mode (< 200 nm in D_{va}) to the droplet mode (500–1000 nm in D_{va}) by coagulation would be too slow with the low concentrations of the present field campaign. Previous studies have shown that chemical reactions in aqueous phases (i.e. fog and cloud droplets and aerosol phase water) usually add much more mass in the droplet mode than in smaller particles and that aqueous-phase sulfate formation is an important process in the atmosphere (Ervens et al., 2011, and references therein). In addition, as shown in Fig. 6c, sulfate correlated well with $CH_2SO_2^+$ and $CH_3SO_2^+$, two HR-AMS ions likely representing methanesulfonic acid (see discussions in Sect. 3.1.1). MSA is known to be produced by oxidation of dimethyl sulfide emitted mainly from oceanic sources and its formation is enhanced by aqueous phase processing (Barnes et al., 2006). For these reasons, we deduce that a large fraction of the droplet mode particles observed during this study likely originated from the San Francisco bay area, where nearby oil refineries (Fig. 1a) are the largest SO_2 sources in Northern California and where aqueous reactions would have been promoted by fogs during morning hours and low clouds.

In contrast, the dominance of the condensation mode in the organic size distribution (Fig. 5b) indicates that condensational growth was the major formation mechanism for organics. Given that m/z 43 and 44 are the two most abundant ions in the mass spectra of the organics at T1 (Fig. 8a), we compared their average size distributions in Fig. 5c. Org 43 (i.e. organic signal at m/z 43) corresponds mainly to the $C_2H_3O^+$ ion, which likely comes from aldehydes or ketones (Ng et al., 2011a). Org 44 is mainly due to the CO_2^+ ion, which is largely associated with carboxylic acids (Alfarra, 2004). The slightly larger mode size of Org 44 compared to that of Org 43 (Fig. 5c) is consistent with the

fact that Org 44 represents organic compounds with a higher level of oxidation and subjected to longer photochemical processing.

3.1.3 Temporal and diurnal variations and implications of aerosol sources and processes at T1

The concentration, chemical composition and size distribution of PM_1 varied dynamically throughout this study (Fig. 2), reflecting the influences from different sources and processes. Organics was the dominant species during the entire study, except during periods of very low PM_1 loading ($< 1\,\mu g\,m^{-3}$), during which the mass fraction of sulfate increased (Fig. 6a). The fact that sulfates dominated the aerosol composition in clean air masses suggests a regional source of sulfate. This is consistent with the larger size distribution of sulfate compared to organics. On the other hand, periods with high PM_1 loading were associated with high mass fraction of organics (Fig. 6d), indicating that episodes of aerosol pollution at the Sierra Nevada foothills were mainly driven by SOA formation (detailed discussions are given in Sect. 3.2). A gradual increase of the particle concentration from 1.5 to $11\,\mu g\,m^{-3}$ was observed between 20 and 28 June 2010 (Fig. 2a). Given that maximum O_3 (in the range 70–80 ppb; Fig. S2c) occurred during these four days, aerosol particles were likely subjected to more intense photochemical processing.

The concentrations and size distributions of the chemical species in PM_1 all showed strong diurnal variations (Fig. 7), which were mainly driven by very consistent wind patterns as well as the formation of secondary aerosols. Indeed, organics and sulfate began to increase at 10:00 and peaked at around 15:00–16:00 (Fig. 7). This time period corresponds to the T0 to T1 transport (Fig. 1b) coupled to photochemical oxidation. Given that the only significant sources of SO_2 identified in the region are the refineries located in the Bay Area (Fig. 1a), the increase of sulfate (mainly in particles smaller than 300 nm in D_{va}, Fig. 7b) in the afternoon may be attributed to the transport of SO_2 and condensation of its photochemical oxidation products. Similarly, the increase of organics during the same period may be due to the transport and subsequent oxida-

tion of anthropogenic (from the Sacramento area) and biogenic (from the vegetation between Sacramento and the T1 site) precursors. We also notice a slight increase of organics and sulfate during the night, with a peak at around 03:00–04:00. This time corresponds to nocturnal downslope flows (Fig. 1b), when a part of the polluted air transported to the Sierra Nevada during the day came back to the foothills. In addition, a decrease of the boundary layer height, thus less dilution, during the night might have played a role in the increase of organic species as well.

New particle formation (NPF) and growth events occurred almost every day during this study (Fig. 2d) and were frequently observed pin Sierra Nevada (Lunden et al., 2006; Creamean et al., 2011). In this study, the particle number concentration shows a sharp increase between 09:00 (2800 particles cm^{-3}) and 14:00 (12 100 particles cm^{-3}) (Fig. 7f), accompanied by the simultaneous increases of organics and sulfate. However, the smallest size measured by our SMPS is 8 nm, while new particles formed by nucleation have generally 1 nm diameter (Holmes, 2007). Therefore, a lag time of 1–2 h is necessary between the formation and the growth of the new particle to a detectable size, and the real nucleation should occur earlier. Moreover, an additional lag of several hours is necessary for new particles to grow until a size detectable by the AMS (minimum 35 nm in D_{va}, corresponding to $\sim$ 25 nm in D_m assuming spherical particle with a density of 1.4 g cm^{-3}). An increase of the organics and sulfate concentrations in the ultrafine mode was observed between 11:00 and 15:00 (Fig. 7). The mass concentration of organics was 8 times higher than that of sulfate at 15:00, indicating a key role played by organics in the new particle growth. We notice that the mass concentrations of both Org 43 (mainly $C_2H_3O^+$) and Org 44 (mainly CO_2^+) in the ultrafine mode increased during this period (Fig. 7c,d). Similarly, increases of Org 43 and 44 in the ultrafine mode were observe during the growth of new particles at Pittsburgh (Zhang et al., 2004, 2005c) and in a Finish Forest (Allan et al., 2006). Since the total increase of these two fragments alone (0.2 µg m^{-3}) is as much as the increase of sulfate during the same period (Fig. 7), oxidized organics appear to have played important roles in growing new particles in the Sierra foothill region. A com-

plete description and the determination of the conditions allowing the formation of new particles and their subsequent growth and the evolution of particle chemistry will be presented in a separate paper.

3.1.4   Bulk properties of organics

Organics, which dominated PM$_1$ composition at T1, were overall oxidized with average O/C=0.44 (range 0.06–0.75), H/C=1.38 (range 1.01–2.09), and OM/OC=1.70 (range 1.19–2.15). The nominal formula of organics at T1 during the CARES was C$_1$H$_{1.38}$N$_{0.004}$O$_{0.44}$. As shown in Fig. 8a, the average organic mass spectrum was dominated by signals at m/z 44 (corresponding mainly to CO$_2^+$) and 43 (mainly C$_2$H$_3$O$^+$). In addition, 55 % of the signal at m/z 57 was contributed by an oxygenated ion – C$_3$H$_5$O$^+$. C$_4$H$_9^+$, which is a dominant ion at m/z 57 in POA from fossil fuel combustion (Mohr et al., 2009) and has been used as an AMS tracer ion for HOA (e.g., Zhang et al., 2005a), accounts for only 0.44 % of the total organic signal, due to minor influence of primary emissions at T1.

The elemental ratios (O/C, H/C and OM/OC) of the organics all have strong diurnal patterns (Fig. 8b–d). For instance, O/C increased from 0.43 to 0.52 between 07:00 and 11:00 (Fig. 8b). Given that the observed increases of O/C coincided with the increases of Org 43 and Org 44 and total organics mass in particles smaller than 300 nm (Fig. 7c,d), daytime condensation of low volatility and oxidized organics onto the surface of pre-exiting particles appeared to be an important mechanism controlling organic aerosol composition and loading in the Sacramento Valley region. The slight decrease of O/C ratio and increase of H/C at 22:00 were likely due to the emissions of primary particles from local sources (Fig. 9i; see Sect. 3.2).

The average O/C ratio of this study was much lower than a field campaign undertaken at Whistler Mountain, an elevated, forested site in Western Canada (Sun et al., 2009). A major reason is that Whistler is frequently subjected to trans-Pacific transport of highly aged aerosols (Sun et al., 2009). In addition, aqueous-phase processing of aerosols in clouds, which could increase the O/C of organics (Ervens et al., 2011),

appeared to be important at Whistler given the frequent cloud coverage and precipitation at the site (Sun et al., 2009). Thus, the O/C determined during the present study may reflect a combination of more oxidized regional aerosols and less aged aerosols associated with daily urban transport.

3.2 Organic aerosol factors and discussions on the sources and processes affecting OA composition

We performed PMF analysis to the high resolution mass spectra of OA and determined the mass spectra, time series and diurnal patterns of three distinct OA factors (Fig. 9), including two different oxygenated OA factors, one of which is more oxidized (OC=0.54) than the other (O/C=0.42), and a hydrocarbon-like OA (HOA, O/C=0.08). A number of previous studies identified more than one OOA factors (Jimenez et al., 2009; Ng et al., 2010). Based on correlations with sulfate and ammonium nitrate, the different OOAs are usually named low volatility and semi-volatile OOA (LV-OOA and SV-OOA, respectively). However, Hildebrandt et al. (2010) identified two OOA factors with similar volatility but different degree of oxidation at a remote coastal site on the island of Crete (Greece). For the present study, preliminary analysis of the thermod-enuder data suggests that both OOA factors appear to be more volatile than sulfate, despite a difference of volatility. Therefore, we will use the terms of "more oxidized" (MO-OOA) and "less oxidized" OOA (LO-OOA) in the forthcoming discussions.

3.2.1 More oxidized OOA (MO-OOA) and association with biogenic emissions

The mass spectrum of MO-OOA is mainly dominated by oxygenated fragments (ions from the $C_xH_yO_1^+$ and $C_xH_yO_2^+$ families) and shows two dominant peaks at m/z 43 (97.4 % is $C_2H_3O^+$) and m/z 44 (97.3 % is CO_2^+). Its O/C ratio (0.54) falls within those of SV-OOA factors identified in world-wide datasets (Jimenez et al., 2009; Ng et al., 2010). Particularly, the mass spectrum of MO-OOA shows many similarities with biogenic SOA from chamber experiments and ambient environments (Shilling et al., 2009;

Kiendler-Scharr et al., 2009; Chen et al., 2009; Chhabra et al., 2010; Sun et al., 2011b). First, the signal of CHO^+ (m/z 29) is clearly enhanced in MO-OOA compared to OOA factors previously published, so are α-pinene SOA (Shilling et al., 2009; Chhabra et al., 2010) and isoprene SOA (Chhabra et al., 2010) from smog chamber experiments and

5   biogenic SOA from plant chamber experiments (Kiendler-Scharr et al., 2009). Second, prominent signals measured in biogenic SOA, e.g., $C_2H_3O^+$ (m/z 43) and $C_3H_6O^+$ (m/z 58) (e.g., Kiendler-Scharr et al., 2009; Shilling et al., 2009), are also enhanced in the MO-OOA spectrum. Finally, the MO-OOA spectrum indicates that the $C_3H_5O^+/C_4H_9^+$ ratio (both at m/z 57) is 40, consistent with observations by Liggio et al. (2010) in that

10   the signal at m/z 57 is dominated by $C_3H_5O^+$ in air masses carrying biogenic SOA, while the $C_3H_5O^+/C_4H_9^+$ ratio decreases down to 0.1 for primary emissions from vehicle exhaust. In addition to the mass spectral signatures, the graph of f_{44} (Org 44/total organic ratio) vs. f_{43} (Org 43/total organic ratio) provides an additional indication that MO-OOA has a biogenic influence (Fig. 12). This triangle plot, first presented by Ng

15   et al. (2010), is a practical way to classify OOA factors identified in different datasets. Factors with different level of oxidation fall in different regions of the triangle plot. The more oxidized LV-OOA usually fall in the upper part of the triangle, while the less oxidized SV-OOA fall in the lower part. The region corresponding to SV-OOA is broad, which indicates that fresh OOAs may have very different mass spectral signatures, de-

20   pending on their source and process, while the upper part of the triangle is much thinner, which indicates that OA composition tends to become more similar after ageing and long oxidation processes. For reference, a second triangle plot corresponding to f_{CO_2} (CO_2^+/total organic ratio) vs. $f_{C_2H_3O}$ ($C_2H_3O^+$/total organic ratio) is given in Fig. S6. The MO-OOA of this study falls very closely to previous OOA factors with biogenic in-

25   fluence (Allan et al., 2006; Cottrell et al., 2008; Sun et al., 2009; Raatikainen et al., 2010; Slowik et al., 2010), while the f_{43}/f_{44} ratio in LO-OOA is substantially higher.

MO-OOA also correlated best with photo-oxidation gases (acetaldehyde, acetic acid, acetone, methyl ethyl ketone, 2-methyl-3-buten-2-ol [MBO], formaldehyde, sum of methacrolein [MACR] and methyl vinyl ketone [MVK]; r^2 in the range 0.5–0.7)

(Fig. 11a). The correlation is especially high with acetone and methanol (r^2 in the range 0.6–0.7), both of which are mainly secondary species with long lifetimes. It is interesting to note that acetone and methanol are very well correlated during this study ($r^2 = 0.87$; Fig. S7), which was also the case during two previous field cam-
paigns at the Blodgett Forest (Schade and Goldstein, 2001, 2006). The production of methanol results mainly from vegetation (Singh et al., 2000), while acetone may have additional influences from anthropogenic primary emissions (Goldstein and Schade, 2000). Moreover, acetone is known to be a significant source of hydroxyl radicals (Singh et al., 1995). Their tight correlation during this study suggests that both VOCs
were mainly produced by biogenic sources and that the relatively high mixing ratio of acetone (2.1 ppb in average, which is consistent with summer measurements performed by Schade and Goldstein, 2006) could be a significant reservoir of hydroxyl radicals. In addition, MO-OOA shows fair correlation with biogenic VOCs (isoprene, monoterpenes; r^2 of 0.3–0.4) and no correlation with tracers of primary emissions from
anthropogenic sources (BC, CO, benzene and derivatives with 2, 3 and 4 substitutions, toluene; $r^2 < 0.2$; Fig. 11a). These results corroborate our hypothesis that MO-OOA was associated with photochemical processing of biogenic precursors. In addition, the high correlation of MO-OOA with MACR and MVK ($r^2 = 0.57$, Fig. 11a), which are the 1st generation oxidation products of isoprene and are formed on a time scale of several
hours (Apel et al., 2002), suggests that this SOA was quite fresh.

3.2.2 Less oxidized OOA (LO-OOA) and association with anthropogenic emissions

The LO-OOA mass spectrum is also dominated by oxygenated fragments, but has a more important contribution of ions from the $C_xH_y^+$ family compared to MO-OOA (Fig. 10a; $C_xH_y^+$ ions account for 48 % in the total signal of the LO-OOA vs. 35 % in that of the MO-OOA). The dominant signal is at m/z 44 (94.1 % is CO_2^+). Even though the f_{44} of this factor is higher than that of the MO-OOA (0.133 vs. 0.109; Fig. 9) and

the Org44/Org43 ratio is also higher (Fig. 12), the O/C ratio of this factor is lower (0.42 vs. 0.54; Fig. 9a, b). This is in contradiction with previous work, which showed that when particles become more oxidized, O/C ratio, f_{44} and Org44/Org43 ratio should all increase (Ng et al., 2010). As mentioned above, the MO-OOA has a high signal of CHO$^+$ at the m/z 29, which accounts for 7.6 % of the total signal in this mass spectrum, compared to 1.0 % in the other OOA factor. This CHO$^+$ signal increases the O/C ratio of the MO-OOA. Moreover, the more important contribution of ions from the $C_xH_y^+$ family to the LO-OOA spectrum also decreases the O/C ratio of this factor.

The LO-OOA shows a strong diurnal pattern, with an increase of the concentration starting at 11:00, reaching the maximum at 16:00, and decreasing during the evening (Fig. 9h). The diurnal pattern observed for the LO-OOA is consistent with a constant southwesterly wind between 09:00 and 21:00 (Fig. 1b), bringing urban outflow from the Sacramento area. Indeed, wind rose corresponding to periods when this OA factor accounted for more than 60 % of the organics mass loading confirms that LO-OOA was dominant when the wind came from the Sacramento area (Fig. S6b). Moreover, the diurnal pattern of LO-OOA is similar to that of sulfate (Fig. 9h), which further supports anthropogenic influences. In summary, the mass spectral signatures of the LO-OOA (e.g., high contribution of ions from the $C_xH_y^+$ family), coupled to its diurnal profile, indicate that this OA factor has anthropogenic influences and corresponds to particles from urban transport.

Taken together, the two OOA factors accounted for 90 % of the total organics mass and 72 % of the PM$_1$ loading. Similarly, the BEARPEX 2007 field campaign also determined that organics were predominantly oxygenated in the Blodgett Forest region (Worton et al., 2011). These observations demonstrate that aerosol population and loading in Northern California are controlled by SOA formation involving both biogenic and anthropogenic emissions.

3.2.3 HOA and association with local traffic emissions

The HOA mass spectrum (Fig. 9c) shows characteristic signals of $C_4H_9^+$ (m/z 57), $C_4H_7^+$ (m/z 55), and ions resulting from the incorporation of CH_2^+ to the hydrocarbon backbone (i.e., the $C_nH_{2n-1}^+$ and $C_nH_{2n+1}^+$ ion series). This OA factor is dominated by ions from the $C_xH_y^+$ family, which account for 83 % of the total signal of HOA (Fig. 10a). Especially, the larger $C_nH_{2n+1}^+$ ($n > 2$) ions in the OA spectra are mostly contributed by HOA, as indicated by their tightly correlations with HOA, but not so with the two OOAs (Fig. S5). A similar behavior was reported for the HOA factor identified during a study at New York City in 2009 (Sun et al., 2011a). The mass spectrum pattern as well as elemental ratios (O/C=0.08, H/C=1.79) of the HOA factor is consistent with those identified during previous field campaigns (e.g., Zhang et al., 2005c; Aiken et al., 2009; Allan et al., 2010; Sun et al., 2011a; Ng et al., 2011b).

The average concentration of HOA is 0.22 µg m^{-3}, accounting for $\sim$ 10 % of total organics over the entire campaign (Table 1). The occasional spikes in HOA (Fig. 9f) were probably due to some local traffic around the sampling site. Overall, the HOA factor shows a slight correlation with tracers of primary pollutants from anthropogenic sources (BC, benzene and derivatives, toluene; r^2 in the range 0.1–0.2; Fig. 11c), and does not appear to be correlated to any other trace gases and VOCs ($r^2 < 0.1$). These poor correlations seem to be due to low concentrations, poor S/N ratios and noisy data. However, the diurnal patterns of CO and BC (two well-known combustion tracers) are similar to that of HOA, all of which show an increase between 06:00–07:00 in the morning and between 21:00–22:00 at evening (Fig. 9i). Thus, this HOA factor seems to mainly come from local primary emissions, instead of transport from upwind urban area.

3.3 Influence of anthropogenic emissions on SOA formation

In order to understand the role played by anthropogenic emissions from Sacramento in the formation of SOA at T1, periods of urban plumes have been compared to other

air masses dominated by biogenic emissions in terms of aerosol concentration, chemical composition, OA components, VOC concentration and average size distribution (Table 1 and Fig. 13). Details on the classification of the three air masses (T0 → T1 transport, northwesterly wind periods and other periods) are given in Sect. 2.3. We notice that the average particle mass concentration was 2.5 times higher in urban plumes ($3.9\,\mu g\,m^{-3}$) than in background air (i.e., during the northwesterly wind period; $1.8\,\mu g\,m^{-3}$). The relative contributions of the OA factors to the total organic mass for each wind pattern are consistent, with urban plumes dominated by the urban transport SOA (LO-OOA), and the northwesterly wind periods dominated by biogenic SOA (MO-OOA). The other periods were dominated by the urban transport SOA, likely because these periods correspond mainly to nocturnal downslope flows, which brought back a part of the polluted air from the Sierra Nevada to the foothills. The average size distributions of organics, sulfate and particle number concentration indicate that organics (mode at around 150–200 nm in D_{va}) and sulfate (around 400 nm in D_{va}) were externally mixed in each air mass (Fig. 13). However, there is one significant difference between these size distributions: the presence of a second mode for sulfate in the range 100–200 nm (D_{va}) during the T0 to T1 transport periods (Fig. 13b). This mode is also visible, but at a lesser extent, during the downslope wind periods, but was absent during the northwesterly wind periods. This was due to the frequent new particle growth events that we observed frequently during the periods of urban plumes and during which low volatile H_2SO_4 and organics condensed onto the surface of small particles.

OA formation in the different air masses can be further investigated using the $\Delta OA/\Delta CO$ ratio in order to take into account of the dilution effect. ΔOA and ΔCO correspond to the organics and CO concentrations above background levels. A background of $0.4\,\mu g\,m^{-3}$ for organics and 75 ppb for CO have been determined based on the averages of the lowest 5 % data over the entire study. Figure 14 shows the relationship between ΔOA and ΔCO during the entire campaign, the diurnal pattern of $\Delta OA/\Delta CO$, and the relationship between ΔOA and ΔCO for different air masses and

Title Page

Abstract | Introduction

Conclusions | References

Tables | Figures

◄ | ►►

◄ | ►

Back | Close

Full Screen / Esc

Printer-friendly Version

Interactive Discussion

periods with different concentrations of biogenic VOCs. Note that ΔOA and ΔCO were not correlated during this study ($r^2 = 0.22$), while the correlation was much higher during a recent field campaign performed at the Blodgett Forest ($r^2 = 0.79$; Worton et al., 2011). The ratio of ΔOA to ΔCO varied between 5–196 $\mu g\,m^{-3}\,ppm^{-1}$ (Fig. 14a), indicating large variations in the change in SOA mass relative to CO. The minimum value of 5 $\mu g\,m^{-3}\,ppm^{-1}$ of this study is very close to the 4 $\mu g\,m^{-3}\,ppm^{-1}$ HOA/CO ratio observed in Pittsburgh (Zhang et al., 2005c), consistent with an influence from primary combustion emissions.

The diurnal pattern of ΔOA/ΔCO shows a gradual increase between 08:00 (36 $\mu g\,m^{-3}\,ppm^{-1}$) and 17:00 (58 $\mu g\,m^{-3}\,ppm^{-1}$). This time period corresponds to the urban plume from T0 to T1 (Fig. 1b), during which the ΔOA/ΔCO increases by 22 $\mu g\,m^{-3}\,ppm^{-1}$. Note that the diurnal pattern of ΔOA/ΔCO shows another gradual increase between 23:00 (30 $\mu g\,m^{-3}\,ppm^{-1}$) and 05:00 (47 $\mu g\,m^{-3}\,ppm^{-1}$). This period corresponds to nocturnal downslope winds (Fig. 1b), during which a part of the polluted air came back from the Sierra Nevada Mountains to the foothills. The increase of ΔOA/ΔCO during this period (17 $\mu g\,m^{-3}\,ppm^{-1}$) is almost the same as during the daytime transport events. These results indicate that the change in SOA mass relative to CO was enhanced during periods when anthropogenic influences increased at T1. An important parameter in the comparison between the different air masses is the photochemical age. Unfortunately, we are not able to determine this parameter with data available at T1 as gas phase toluene and benzene measured by PTR/MS are too noisy, while the NO_x/NO_y ratio cannot be used, because NO_x was not measured at T1. However, a basic comparison with previous studies may be done using the change in organic carbon mass relative to CO (ΔOC/ΔCO). This ratio is determined using organics and CO concentrations above background, and the OM/OC ratio. The average ΔOC/ΔCO for the entire study was 20.9 $\mu g\,C\,m^{-3}\,ppm^{-1}$, while the average ratio for each air mass was 25.3 (T0 to T1 transport), 16.8 (northwesterly wind) and 20.8 $\mu g\,C\,m^{-3}\,ppm^{-1}$ (other periods). Sullivan et al. (2006) and Weber et al. (2007) showed that the change in water soluble organic carbon mass relative to

CO (ΔWSOC/ΔCO) approached a constant value in the range 32–35 μg C m^{-3} ppm^{-1} in plumes that had advection times longer than 30 h, while de Gouw et al. (2008) found similar results for ΔOC/ΔCO. During this study, the highest value of ΔOC/ΔCO (25.3 μg C m^{-3} ppm^{-1} for periods of urban transport) would correspond to a photochemical age of $\sim$ 15–20 h, according to the relationship between ΔOC/ΔCO (or ΔWSOC/ΔCO) and photochemical age (Sullivan et al., 2006; Weber et al., 2007; de Gouw et al., 2008). This time period is much longer than the time needed for particles to be transported from T0 to T1, which is $\sim$ 3 h according to the comparison of AMS data from these two sites. This result suggests that during periods of T0 to T1 transport, anthropogenic precursors emitted at Sacramento were transported with particles which were formed upstream (i.e., between San Francisco and Sacramento; Fig. 1a) and which were already subjected to a long photochemical processing.

The scatterplots on Fig. 14c–e suggest that the increase of anthropogenic influences is not sufficient to explain the enhancement of the SOA formation and that the slope of ΔOA vs. ΔCO depends dramatically on the amount of biogenic VOCs present during these periods. To calculate the sum of biogenic VOCs, we took into account isoprene, monoterpenes, MBO and methyl chavicol, knowing that isoprene was by far the most abundant biogenic VOC measured during this study (82 % of the total biogenic VOCs in average). However, note that the temporal variations of the different biogenic VOCs are very different (Fig. S2), isoprene being dominant during the day while monoterpenes were higher during the night and obviously transported during the downslope flows from the Sierra Nevada to the foothills. We notice that during the transport periods from T0 to T1 (Fig. 14c), the slope of ΔOA vs. ΔCO increases by a factor of 3 when the sum of biogenic VOCs was higher than 2 ppb, compared to periods when the mixing ratio was lower than 0.7 ppb (77 vs. 28 μg m^{-3} ppm^{-1}). This change in SOA mass relative to CO is approximately the same as that during the downslope flows (71 μg m^{-3} ppm^{-1}; Fig. 14e) when anthropogenic influences were still present, but is much higher than during the northwesterly wind periods (40 μg m^{-3} ppm^{-1}; Fig. 14d) dominated by biogenic SOAs.

In summary, these results suggest that the SOA formation was enhanced when anthropogenic influences increased at Cool, but only if significant amounts of biogenic precursors were present. The observations from this study also support the hypothesis that the interaction between anthropogenic and biogenic precursors enhances the SOA formation (de Gouw et al., 2005; Volkamer et al., 2006; Weber et al., 2007; Kleinman et al., 2008).

4 Conclusions

An HR-ToF-AMS and an SMPS were deployed at Cool, CA, the T1 rural site of the CARES field campaign in June 2010. With this set of instruments, the mass concentration, chemical composition and size distributions of submicron aerosols were characterized. The sampling site is located in a forested region, at the foothill of the Sierra Nevada Mountains, where biogenic emissions are periodically mixed with urban outflow transported by consistent southwest winds from Sacramento. The average mass loading during the entire campaign was $3.0\,\mu g\,m^{-3}$ on average, with organics (80 % of the total PM_1 mass) being the dominant component followed by sulfate (9.9 %), ammonium (4.5 %), nitrate (3.6 %), black carbon (1.6 %), and chloride (0.1 %). The amount of ammonium appeared sufficient to fully neutralize observed anions (sum of $SO_4^{2-} + NO_3^- + Cl^-$), indicating that sulfate was mainly present in the form of $(NH_4)_2SO_4$ at T1. The average size distribution indicates that sulfate was mainly in the accumulation mode (D_{va} 200–600 nm), while organics showed broader distributions that extend to smaller sizes. The size distribution of nitrate, which was a minor component of PM_1 (4 %), followed the same trend as organics due to the fact that a significant fraction of the nitrate signal comes from organonitrates, while that of ammonium followed the same trend as sulfate due to full neutralization of anions. New particle formation and growth events were observed almost every day with the SMPS. Our results showed that organics and, to a lesser extent, sulfate played a key-role in the new particle growth. Three OA factors were identified by PMF analysis of the high resolution mass spectra:

two different OOA components (90 % of total organics) and a HOA (10 %). The more oxidized MO-OOA (O/C=0.54) was identified as biogenically influenced SOA, while the less oxidized LO-OOA (O/C=0.42) corresponded to anthropogenically influenced SOA (e.g., from the Sacramento area). The HOA factor corresponded mainly to primary emissions from local traffic. While the diurnal variation patterns of sulfate and LO-OOA both showed daytime increases consistent with impacts from urban transport, the time series of these two species poorly correlated, indicating different source regions of their precursor species and formation mechanisms.

23 periods of urban plumes from T0 (Sacramento) to T1 (Cool) were identified using the WRF-Chem model. The comparison of the urban plumes with other air masses dominated by biogenic SOAs showed two major differences: a much higher mass loading during the T0 to T1 transport periods than during northwesterly wind periods (3.9 vs. 1.8 μg m^{-3}) and the presence of a second mode of sulfate in small sizes (D_{va} 100–200 nm) in urban plumes, due to the frequent occurrence of new particle growth events that we observed during the T0 to T1 transport periods. The average chemical composition of aerosols, however, was overall similar in the different types of air mass. The increase ratio of OA concentration relative to the increase of CO (ΔOA/ΔCO) varied in the range 5–196 μg m^{-3} ppm^{-1}. The highest values of ΔOA/ΔCO were reached when urban plumes arrived at T1 in the presence of a high concentration of biogenic VOCs (77 μg m^{-3} ppm^{-1} when biogenic VOCs are higher than 2 ppb vs. 28 μg m^{-3} ppm^{-1} when biogenic VOCs are lower than 0.7 ppb). This change in SOA mass relative to CO was also much higher than that in other air masses dominated by biogenic SOA (40 μg m^{-3} ppm^{-1}). This observation suggests that SOA formation is enhanced when urban emissions from Sacramento arrive at T1 and interact with biogenic precursors.

Supplementary material related to this article is available online at: http://www.atmos-chem-phys-discuss.net/12/5601/2012/ acpd-12-5601-2012-supplement.pdf.

Title Page

Abstract	Introduction
Conclusions	References
Tables	Figures

◄◄	►►
◄	►
Back	Close

Full Screen / Esc

Printer-friendly Version

Interactive Discussion

References

Aiken, A. C., Decarlo, P. F., Kroll, J. H., Worsnop, D. R., Huffman, J. A., Docherty, K. S., Ulbrich, I. M., Mohr, C., Kimmel, J. R., Sueper, D., Sun, Y., Zhang, Q., Trimborn, A., Northway, M., Ziemann, P. J., Canagaratna, M. R., Onasch, T. B., Alfarra, M. R., Prevot, A. S. H., Dommen, J., Duplissy, J., Metzger, A., Baltensperger, U., and Jimenez, J. L.: O/C and OM/OC ratios of primary, secondary, and ambient organic aerosols with high-resolution time-of-flight aerosol mass spectrometry, Environ. Sci. Technol., 42, 4478–4485, doi:10.1021/es703009q, 2008.

Aiken, A. C., Salcedo, D., Cubison, M. J., Huffman, J. A., DeCarlo, P. F., Ulbrich, I. M., Docherty, K. S., Sueper, D., Kimmel, J. R., Worsnop, D. R., Trimborn, A., Northway, M., Stone, E. A., Schauer, J. J., Volkamer, R. M., Fortner, E., de Foy, B., Wang, J., Laskin, A., Shutthanandan, V., Zheng, J., Zhang, R., Gaffney, J., Marley, N. A., Paredes-Miranda, G., Arnott, W. P., Molina, L. T., Sosa, G., and Jimenez, J. L.: Mexico City aerosol analysis during MILAGRO using high resolution aerosol mass spectrometry at the urban supersite (T0) – Part 1: Fine particle composition and organic source apportionment, Atmos. Chem. Phys., 9, 6633–6653, doi:10.5194/acp-9-6633-2009, 2009.

Alfarra, M. R.: Insights Into Atmospheric Organic Aerosols Using An Aerosol Mass Spectrometer, PhD Dissertation Thesis, Department of Chemical Engineering, University of Manchester, Manchester, UK, 2004.

Alfarra, M. R., Coe, H., Allan, J. D., Bower, K. N., Boudries, H., Canagaratna, M. R., Jimenez, J. L., Jayne, J. T., Garforth, A. A., Li, S. M., and Worsnop, D. R.: Characterization of urban and rural organic particulate in the lower Fraser valley using two aerodyne aerosol mass spectrometers, Atmos. Environ., 38, 5745–5758, doi:10.1016/j.atmosenv.2004.01.054, 2004.

Alfarra, M. R., Prevot, A. S. H., Szidat, S., Sandradewi, J., Weimer, S., Lanz, V. A., Schreiber, D., Mohr, M., and Baltensperger, U.: Identification of the Mass Spectral Signature of Organic Aerosols from Wood Burning Emissions, Environ. Sci. Technol., 41, 5770–5777, doi:10.1021/es062289b, 2007.

Allan, J. D., Delia, A. E., Coe, H., Bower, K. N., Alfarra, M. R., Jimenez, J. L., Middlebrook, A. M., Drewnick, F., Onasch, T. B., Canagaratna, M. R., Jayne, J. T., and Worsnop, D. R.: A generalised method for the extraction of chemically resolved mass spectra from aerodyne aerosol mass spectrometer data, J. Aerosol. Sci., 35, 909–922, doi:10.1016/j.jaerosci.2004.02.007, 2004.

Allan, J. D., Alfarra, M. R., Bower, K. N., Coe, H., Jayne, J. T., Worsnop, D. R., Aalto, P. P., Kulmala, M., Hyötyläinen, T., Cavalli, F., and Laaksonen, A.: Size and composition measurements of background aerosol and new particle growth in a Finnish forest during QUEST 2 using an Aerodyne Aerosol Mass Spectrometer, Atmos. Chem. Phys., 6, 315–327, doi:10.5194/acp-6-315-2006, 2006.

Allan, J. D., Williams, P. I., Morgan, W. T., Martin, C. L., Flynn, M. J., Lee, J., Nemitz, E., Phillips, G. J., Gallagher, M. W., and Coe, H.: Contributions from transport, solid fuel burning and cooking to primary organic aerosols in two UK cities, Atmos. Chem. Phys., 10, 647–668, doi:10.5194/acp-10-647-2010, 2010.

Apel, E. C., Riemer, D. D., Hills, A., Baugh, W., Orlando, J., Faloona, I., Tan, D., Brune, W., Lamb, B., Westberg, H., Carroll, M. A., Thornberry, T., and Geron, C. D.: Measurement and interpretation of isoprene fluxes and isoprene, methacrolein, and methyl vinyl ketone mixing ratios at the PROPHET site during the 1998 Intensive, J. Geophys. Res., 107, 4034, doi:10.1029/2000jd000225, 2002.

Barnes, I., Hjorth, J., and Mihalopoulos, N.: Dimethyl sulfide and dimethyl sulfoxide and their oxidation in the atmosphere, Chem. Rev., 106, 940–975, 2006.

Birmili, W., Stratmann, F., Wiedensohler, A., Covert, D., Russell, L. M., and Berg, O.: Determination of differential mobility analyzer transfer functions using identical instruments in series, Aerosol Sci. Technol., 27, 215–223, doi:10.1080/02786829708965468, 1997.

Bond, T. C. and Bergstrom, R. W.: Light absorption by carbonaceous particles: an investigative review, Aerosol Sci. Technol., 40, 27–67, 2006.

Bouvier-Brown, N. C., Goldstein, A. H., Gilman, J. B., Kuster, W. C., and de Gouw, J. A.: In-situ ambient quantification of monoterpenes, sesquiterpenes, and related oxygenated compounds during BEARPEX 2007: implications for gas- and particle-phase chemistry, Atmos. Chem. Phys., 9, 5505–5518, doi:10.5194/acp-9-5505-2009, 2009.

Cahill, T. M., Seaman, V. Y., Charles, M. J., Holzinger, R., and Goldstein, A. H.: Secondary organic aerosols formed from oxidation of biogenic volatile organic compounds in the Sierra Nevada Mountains of California, J. Geophys. Res.-Atmos., 111, D16312,

doi:10.1029/2006jd007178, 2006.

Canagaratna, M. R., Jayne, J. T., Jimenez, J. L., Allan, J. D., Alfarra, M. R., Zhang, Q., Onasch, T. B., Drewnick, F., Coe, H., Middlebrook, A., Delia, A., Williams, L. R., Trimborn, A. M., Northway, M. J., DeCarlo, P. F., Kolb, C. E., Davidovits, P., and Worsnop, D. R.: Chemical and microphysical characterization of ambient aerosols with the aerodyne aerosol mass spectrometer, Mass Spectrom. Rev., 26, 185–222, doi:10.1002/mas.20115, 2007.

Chen, Q., Farmer, D. K., Schneider, J., Zorn, S. R., Heald, C. L., Karl, T. G., Guenther, A., Allan, J. D., Robinson, N., Coe, H., Kimmel, J. R., Pauliquevis, T., Borrmann, S., Po uml schl, U., Andreae, M. O., Artaxo, P., Jimenez, J. L., and Martin, S. T.: Mass spectral characterization of submicron biogenic organic particles in the Amazon Basin, Geophys. Res. Lett., 36, L20806, doi:10.1029/2009gl039880, 2009.

Chhabra, P. S., Flagan, R. C., and Seinfeld, J. H.: Elemental analysis of chamber organic aerosol using an aerodyne high-resolution aerosol mass spectrometer, Atmos. Chem. Phys., 10, 4111–4131, doi:10.5194/acp-10-4111-2010, 2010.

Clausnitzer, H. and Singer, M. J.: Respirable-dust production from agricultural operations in the Sacramento Valley, California, J. Environ. Qual., 25, 877–884, 1996.

Cottrell, L. D., Griffin, R. J., Jimenez, J. L., Zhang, Q., Ulbrich, I., Ziemba, L. D., Beckman, P. J., Sive, B. C., and Talbot, R. W.: Submicron particles at Thompson Farm during ICARTT measured using aerosol mass spectrometry, J. Geophys. Res.-Atmos., 113, D08212, doi:10.1029/2007jd009192, 2008.

Creamean, J. M., Ault, A. P., Ten Hoeve, J. E., Jacobson, M. Z., Roberts, G. C., and Prather, K. A.: Measurements of Aerosol Chemistry during New Particle Formation Events at a Remote Rural Mountain Site, Environ. Sci. Technol., 45, 8208–8216, doi:10.1021/es103692f, 2011.

de Gouw, J. and Warneke, C.: Measurements of volatile organic compounds in the earths atmosphere using proton-transfer-reaction mass spectrometry, Mass Spectrom. Rev., 26, 223–257, 2007.

de Gouw, J. A., Middlebrook, A. M., Warneke, C., Goldan, P. D., Kuster, W. C., Roberts, J. M., Fehsenfeld, F. C., Worsnop, D. R., Canagaratna, M. R., Pszenny, A. A. P., Keene, W. C., Marchewka, M., Bertman, S. B., and Bates, T. S.: Budget of organic carbon in a polluted atmosphere: Results from the New England Air Quality Study in 2002, J. Geophys. Res.-Atmos., 110, D16305, doi:10.1029/2004jd005623, 2005.

de Gouw, J. A., Brock, C. A., Atlas, E. L., Bates, T. S., Fehsenfeld, F. C., Goldan, P. D., Holloway, J. S., Kuster, W. C., Lerner, B. M., Matthew, B. M., Middlebrook, A. M., Onasch, T. B., Peltier,

Submicron particles influenced by emissions

A. Setyan et al.

Title Page

Abstract | Introduction

Conclusions | References

Tables | Figures

◄ | ►

◄ | ►

Back | Close

Full Screen / Esc

Printer-friendly Version

Interactive Discussion

R. E., Quinn, P. K., Senff, C. J., Stohl, A., Sullivan, A. P., Trainer, M., Warneke, C., Weber, R. J., and Williams, E. J.: Sources of particulate matter in the northeastern United States in summer: 1. Direct emissions and secondary formation of organic matter in urban plumes, J. Geophys. Res.-Atmos., 113, D08301, doi:10.1029/2007jd009243, 2008.

5 DeCarlo, P. F., Slowik, J. G., Worsnop, D. R., Davidovits, P., and Jimenez, J. L.: Particle morphology and density characterization by combined mobility and aerodynamic diameter measurements. Part 1: Theory, Aerosol Sci. Technol., 38, 1185–1205, 2004.

DeCarlo, P. F., Kimmel, J. R., Trimborn, A., Northway, M. J., Jayne, J. T., Aiken, A. C., Gonin, M., Fuhrer, K., Horvath, T., Docherty, K. S., Worsnop, D. R., and Jimenez, J. L.:
10 Field-deployable, high-resolution, time-of-flight aerosol mass spectrometer, Anal. Chem., 78, 8281-8289, 10.1021/ac061249n, 2006.

Dillon, M. B., Lamanna, M. S., Schade, G. W., Goldstein, A. H., and Cohen, R. C.: Chemical evolution of the Sacramento urban plume: Transport and oxidation, J. Geophys. Res.-Atmos., 107, 4045, doi:10.1029/2001jd000969, 2002.

15 Dzepina, K., Volkamer, R. M., Madronich, S., Tulet, P., Ulbrich, I. M., Zhang, Q., Cappa, C. D., Ziemann, P. J., and Jimenez, J. L.: Evaluation of recently-proposed secondary organic aerosol models for a case study in Mexico City, Atmos. Chem. Phys., 9, 5681–5709, doi:10.5194/acp-9-5681-2009, 2009.

Ervens, B., Turpin, B. J., and Weber, R. J.: Secondary organic aerosol formation in cloud
20 droplets and aqueous particles (aqSOA): a review of laboratory, field and model studies, Atmos. Chem. Phys., 11, 11069–11102, doi:10.5194/acp-11-11069-2011, 2011.

Farmer, D. K., Matsunaga, A., Docherty, K. S., Surratt, J. D., Seinfeld, J. H., Ziemann, P. J., and Jimenez, J. L.: Response of an aerosol mass spectrometer to organonitrates and organosulfates and implications for atmospheric chemistry, Proc. Natl. Acad. Sci. USA, 107,
25 6670–6675, doi:10.1073/pnas.0912340107, 2010.

Farmer, D. K., Kimmel, J. R., Phillips, G., Docherty, K. S., Worsnop, D. R., Sueper, D., Nemitz, E., and Jimenez, J. L.: Eddy covariance measurements with high-resolution time-of-flight aerosol mass spectrometry: a new approach to chemically resolved aerosol fluxes, Atmos. Meas. Tech., 4, 1275–1289, doi:10.5194/amt-4-1275-2011, 2011.

30 Fast, J. D., Gustafson Jr., W. I., Berg, L. K., Shaw, W. J., Pekour, M., Shrivastava, M., Barnard, J. C., Ferrare, R. A., Hostetler, C. A., Hair, J. A., Erickson, M., Jobson, B. T., Flowers, B., Dubey, M. K., Springston, S., Pierce, R. B., Dolislager, L., Pederson, J., and Zaveri, R. A.: Transport and mixing patterns over Central California during the carbonaceous aerosol and

Title Page

Abstract	Introduction
Conclusions	References
Tables	Figures

⏮ ⏭

◀ ▶

Back Close

Full Screen / Esc

Printer-friendly Version

Interactive Discussion

radiative effects study (CARES), Atmos. Chem. Phys., 12, 1759–1783, doi:10.5194/acp-12-1759-2012, 2012.

Ge, X., Zhang, Q., Sun, Y., and Ruehl, C. R.: Impact of aqueous-phase processing on aerosol chemistry in Fresno, California, during Wintertime, Environ. Chem., submitted, 2012.

Goldstein, A. H. and Schade, G. W.: Quantifying biogenic and anthropogenic contributions to acetone mixing ratios in a rural environment, Atmos. Environ., 34, 4997–5006, 2000.

Goldstein, A. H., Hultman, N. E., Fracheboud, J. M., Bauer, M. R., Panek, J. A., Xu, M., Qi, Y., Guenther, A. B., and Baugh, W.: Effects of climate variability on the carbon dioxide, water, and sensible heat fluxes above a ponderosa pine plantation in the Sierra Nevada (CA), Agric. For. Meteorol., 101, 113–129, 2000.

Goldstein, A. H., Koven, C. D., Heald, C. L., and Fung, I. Y.: Biogenic carbon and anthropogenic pollutants combine to form a cooling haze over the Southeastern United States, Proc. Natl. Acad. Sci., 106, 8835–8840, 2009.

Hallquist, M., Wenger, J. C., Baltensperger, U., Rudich, Y., Simpson, D., Claeys, M., Dommen, J., Donahue, N. M., George, C., Goldstein, A. H., Hamilton, J. F., Herrmann, H., Hoffmann, T., Iinuma, Y., Jang, M., Jenkin, M. E., Jimenez, J. L., Kiendler-Scharr, A., Maenhaut, W., McFiggans, G., Mentel, Th. F., Monod, A., Prévôt, A. S. H., Seinfeld, J. H., Surratt, J. D., Szmigielski, R., and Wildt, J.: The formation, properties and impact of secondary organic aerosol: current and emerging issues, Atmos. Chem. Phys., 9, 5155–5236, doi:10.5194/acp-9-5155-2009, 2009.

Hildebrandt, L., Engelhart, G. J., Mohr, C., Kostenidou, E., Lanz, V. A., Bougiatioti, A., DeCarlo, P. F., Prevot, A. S. H., Baltensperger, U., Mihalopoulos, N., Donahue, N. M., and Pandis, S. N.: Aged organic aerosol in the Eastern Mediterranean: the Finokalia Aerosol Measurement Experiment – 2008, Atmos. Chem. Phys., 10, 4167–4186, doi:10.5194/acp-10-4167-2010, 2010.

Holmes, N. S.: A review of particle formation events and growth in the atmosphere in the various environments and discussion of mechanistic implications, Atmos. Environ., 41, 2183–2201, 2007.

Holzinger, R., Lee, A., Paw, K. T., and Goldstein, U. A. H.: Observations of oxidation products above a forest imply biogenic emissions of very reactive compounds, Atmos. Chem. Phys., 5, 67–75, doi:10.5194/acp-5-67-2005, 2005.

Hoyle, C. R., Boy, M., Donahue, N. M., Fry, J. L., Glasius, M., Guenther, A., Hallar, A. G., Huff Hartz, K., Petters, M. D., Petäjä, T., Rosenoern, T., and Sullivan, A. P.: A review of the

anthropogenic influence on biogenic secondary organic aerosol, Atmos. Chem. Phys., 11, 321–343, doi:10.5194/acp-11-321-2011, 2011.

IPCC: Summary for Policymakers, in: Climate Change 2007: The Physical Science Basis. Contribution of Working Group I to the Fourth Assessment Report of the Intergovernmental Panel on Climate Change, edited by: Solomon, S., Qin, D., Manning, M., Chen, Z., Marquis, M., Averyt, K. B., M.Tignor, and Miller, H. L., Cambridge University Press, Cambridge, UK and New York, NY, USA, 2007.

Jayne, J. T., Leard, D. C., Zhang, X. F., Davidovits, P., Smith, K. A., Kolb, C. E., and Worsnop, D. R.: Development of an aerosol mass spectrometer for size and composition analysis of submicron particles, Aerosol Sci. Technol., 33, 49–70, 2000.

Jimenez, J. L., Canagaratna, M. R., Donahue, N. M., Prevot, A. S. H., Zhang, Q., Kroll, J. H., DeCarlo, P. F., Allan, J. D., Coe, H., Ng, N. L., Aiken, A. C., Docherty, K. S., Ulbrich, I. M., Grieshop, A. P., Robinson, A. L., Duplissy, J., Smith, J. D., Wilson, K. R., Lanz, V. A., Hueglin, C., Sun, Y. L., Tian, J., Laaksonen, A., Raatikainen, T., Rautiainen, J., Vaattovaara, P., Ehn, M., Kulmala, M., Tomlinson, J. M., Collins, D. R., Cubison, M. J., Dunlea, E. J., Huffman, J. A., Onasch, T. B., Alfarra, M. R., Williams, P. I., Bower, K., Kondo, Y., Schneider, J., Drewnick, F., Borrmann, S., Weimer, S., Demerjian, K., Salcedo, D., Cottrell, L., Griffin, R., Takami, A., Miyoshi, T., Hatakeyama, S., Shimono, A., Sun, J. Y., Zhang, Y. M., Dzepina, K., Kimmel, J. R., Sueper, D., Jayne, J. T., Herndon, S. C., Trimborn, A. M., Williams, L. R., Wood, E. C., Middlebrook, A. M., Kolb, C. E., Baltensperger, U., and Worsnop, D. R.: Evolution of Organic Aerosols in the Atmosphere, Science, 326, 1525–1529, doi:10.1126/science.1180353, 2009.

Kanakidou, M., Tsigaridis, K., Dentener, F. J., and Crutzen, P. J.: Human-activity-enhanced formation of organic aerosols by biogenic hydrocarbon oxidation, J. Geophys. Res., 105, 9243–9354, 2000.

Kanakidou, M., Seinfeld, J. H., Pandis, S. N., Barnes, I., Dentener, F. J., Facchini, M. C., Van Dingenen, R., Ervens, B., Nenes, A., Nielsen, C. J., Swietlicki, E., Putaud, J. P., Balkanski, Y., Fuzzi, S., Horth, J., Moortgat, G. K., Winterhalter, R., Myhre, C. E. L., Tsigaridis, K., Vignati, E., Stephanou, E. G., and Wilson, J.: Organic aerosol and global climate modelling: a review, Atmos. Chem. Phys., 5, 1053–1123, doi:10.5194/acp-5-1053-2005, 2005.

Kiendler-Scharr, A., Zhang, Q., Hohaus, T., Kleist, E., Mensah, A., Mentel, T. F., Spindler, C., Uerlings, R., Tillmann, R., and Wildt, J.: Aerosol Mass Spectrometric Features of Biogenic SOA: Observations from a Plant Chamber and in Rural Atmospheric Environments, Environ.

Submicron particles influenced by emissions

A. Setyan et al.

Title Page

Abstract	Introduction
Conclusions	References
Tables	Figures

|◄ | ►|

◄ | ►

Back | Close

Full Screen / Esc

Printer-friendly Version

Interactive Discussion

Sci. Technol., 43, 8166–8172, doi:10.1021/es901420b, 2009.

Kleinman, L. I., Daum, P. H., Lee, Y.-N., Senum, G. I., Springston, S. R., Wang, J., Berkowitz, C., Hubbe, J., Zaveri, R. A., Brechtel, F. J., Jayne, J., Onasch, T. B., and Worsnop, D.: Aircraft observations of aerosol composition and ageing in New England and Mid-Atlantic States during the summer 2002 New England Air Quality Study field campaign, J. Geophys. Res., 112, D09310, doi:10.1029/2006jd007786, 2007.

Kleinman, L. I., Springston, S. R., Daum, P. H., Lee, Y.-N., Nunnermacker, L. J., Senum, G. I., Wang, J., Weinstein-Lloyd, J., Alexander, M. L., Hubbe, J., Ortega, J., Canagaratna, M. R., and Jayne, J.: The time evolution of aerosol composition over the Mexico City plateau, Atmos. Chem. Phys., 8, 1559–1575, doi:10.5194/acp-8-1559-2008, 2008.

Kuwata, M., Zorn, S. R., and Martin, S. T.: Using Elemental Ratios to Predict the Density of Organic Material Composed of Carbon, Hydrogen, and Oxygen, Environ. Sci. Technol., 46, 787–794, doi:10.1021/es202525q, 2011.

Liggio, J., Li, S. M., Vlasenko, A., Sjostedt, S., Chang, R., Shantz, N., Abbatt, J., Slowik, J. G., Bottenheim, J. W., Brickell, P. C., Stroud, C., and Leaitch, W. R.: Primary and secondary organic aerosols in urban air masses intercepted at a rural site, J. Geophys. Res.-Atmos., 115, D21305, doi:10.1029/2010jd014426, 2010.

Lunden, M. M., Black, D. R., McKay, M., Revzan, K. L., Goldstein, A. H., and Brown, N. J.: Characteristics of fine particle growth events observed above a forested ecosystem in the Sierra Nevada Mountains of California, Aerosol Sci. Technol., 40, 373-388, 10.1080/02786820600631896, 2006.

Mahowald, N.: Aerosol Indirect Effect on Biogeochemical Cycles and Climate, Science, 334, 794–796, doi:10.1126/science.1207374, 2011.

Matthew, B. M., Middlebrook, A. M., and Onasch, T. B.: Collection efficiencies in an Aerodyne Aerosol Mass Spectrometer as a function of particle phase for laboratory generated aerosols, Aerosol Sci. Technol., 42, 884–898, 2008.

Middlebrook, A. M., Bahreini, R., Jimenez, J. L., and Canagaratna, M. R.: Evaluation of composition-dependent collection efficiencies for the aerodyne aerosol mass spectrometer using field data, Aerosol Sci. Technol., 46, 258–271, 2012.

Mohr, C., Huffman, J. A., Cubison, M. J., Aiken, A. C., Docherty, K. S., Kimmel, J. R., Ulbrich, I. M., Hannigan, M., and Jimenez, J. L.: Characterization of Primary Organic Aerosol Emissions from Meat Cooking, Trash Burning, and Motor Vehicles with High-Resolution Aerosol Mass Spectrometry and Comparison with Ambient and Chamber Observations, Environ. Sci.

Submicron particles influenced by emissions

A. Setyan et al.

Title Page

Abstract | Introduction

Conclusions | References

Tables | Figures

◄ | ►|

◄ | ►

Back | Close

Full Screen / Esc

Printer-friendly Version

Interactive Discussion

Technol., 43, 2443–2449, doi:10.1021/es8011518, 2009.

Murphy, J. G., Day, D. A., Cleary, P. A., Wooldridge, P. J., Millet, D. B., Goldstein, A. H., and Cohen, R. C.: The weekend effect within and downwind of Sacramento – Part 1: Observations of ozone, nitrogen oxides, and VOC reactivity, Atmos. Chem. Phys., 7, 5327–5339, doi:10.5194/acp-7-5327-2007, 2007.

Ng, N. L., Canagaratna, M. R., Zhang, Q., Jimenez, J. L., Tian, J., Ulbrich, I. M., Kroll, J. H., Docherty, K. S., Chhabra, P. S., Bahreini, R., Murphy, S. M., Seinfeld, J. H., Hildebrandt, L., Donahue, N. M., DeCarlo, P. F., Lanz, V. A., Prévôt, A. S. H., Dinar, E., Rudich, Y., and Worsnop, D. R.: Organic aerosol components observed in Northern Hemispheric datasets from Aerosol Mass Spectrometry, Atmos. Chem. Phys., 10, 4625–4641, doi:10.5194/acp-10-4625-2010, 2010.

Ng, N. L., Canagaratna, M. R., Jimenez, J. L., Chhabra, P. S., Seinfeld, J. H., and Worsnop, D. R.: Changes in organic aerosol composition with aging inferred from aerosol mass spectra, Atmos. Chem. Phys., 11, 6465–6474, doi:10.5194/acp-11-6465-2011, 2011a.

Ng, N. L., Canagaratna, M. R., Jimenez, J. L., Zhang, Q., Ulbrich, I. M., and Worsnop, D. R.: Real-Time Methods for Estimating Organic Component Mass Concentrations from Aerosol Mass Spectrometer Data, Environ. Sci. Technol., 45, 910–916, 10.1021/es102951k, 2011b.

Paatero, P. and Tapper, U.: Positive matrix factorization – a nonnegative factor model with optimal utilization of error-estimates of data values, Environmetrics, 5, 111–126, 1994.

Pope, C. A., Ezzati, M., and Dockery, D. W.: Fine-particulate air pollution and life expectancy in the United States, New Engl. J. Med., 360, 376–386, 2009.

Raatikainen, T., Vaattovaara, P., Tiitta, P., Miettinen, P., Rautiainen, J., Ehn, M., Kulmala, M., Laaksonen, A., and Worsnop, D. R.: Physicochemical properties and origin of organic groups detected in boreal forest using an aerosol mass spectrometer, Atmos. Chem. Phys., 10, 2063–2077, doi:10.5194/acp-10-2063-2010, 2010.

Rollins, A. W., Fry, J. L., Hunter, J. F., Kroll, J. H., Worsnop, D. R., Singaram, S. W., and Cohen, R. C.: Elemental analysis of aerosol organic nitrates with electron ionization high-resolution mass spectrometry, Atmos. Meas. Tech., 3, 301–310, doi:10.5194/amt-3-301-2010, 2010.

Schade, G. W. and Goldstein, A. H.: Fluxes of oxygenated volatile organic compounds from a ponderosa pine plantation, J. Geophys. Res.-Atmos., 106, 3111–3123, 2001.

Schade, G. W., and Goldstein, A. H.: Seasonal measurements of acetone and methanol: Abundances and implications for atmospheric budgets, Glob. Biogeochem. Cycle, 20, GB1011,

Title Page

Abstract | Introduction

Conclusions | References

Tables | Figures

|◄ | ►|

◄ | ►

Back | Close

Full Screen / Esc

Printer-friendly Version

Interactive Discussion

doi:10.1029/2005GB002566, 2006.

Seinfeld, J. H. and Pandis, S. N.: Atmospheric Chemistry and Physics: from Air Pollution to Climate Change, 2nd edn., John Wiley & Sons, Hoboken, 1232 pp., 2006.

Shilling, J. E., Chen, Q., King, S. M., Rosenoern, T., Kroll, J. H., Worsnop, D. R., DeCarlo, P. F., Aiken, A. C., Sueper, D., Jimenez, J. L., and Martin, S. T.: Loading-dependent elemental composition of α-pinene SOA particles, Atmos. Chem. Phys., 9, 771–782, doi:10.5194/acp-9-771-2009, 2009.

Singh, H., Chen, Y., Tabazadeh, A., Fukui, Y., Bey, I., Yantosca, R., Jacob, D., Arnold, F., Wohlfrom, K., Atlas, E., Flocke, F., Blake, D., Blake, N., Heikes, B., Snow, J., Talbot, R., Gregory, G., Sachse, G., Vay, S., and Kondo, Y.: Distribution and fate of selected oxygenated organic species in the troposphere and lower stratosphere over the Atlantic, J. Geophys. Res., 105, 3795–3805, doi:10.1029/1999jd900779, 2000.

Singh, H. B., Kanakidou, M., Crutzen, P. J., and Jacob, D. J.: High-concentrations and photo-chemical fate of oxygenated hydrocarbons in the global troposphere, Nature, 378, 50–54, 1995.

Slowik, J. G., Stroud, C., Bottenheim, J. W., Brickell, P. C., Chang, R. Y.-W., Liggio, J., Makar, P. A., Martin, R. V., Moran, M. D., Shantz, N. C., Sjostedt, S. J., van Donkelaar, A., Vlasenko, A., Wiebe, H. A., Xia, A. G., Zhang, J., Leaitch, W. R., and Abbatt, J. P. D.: Characterization of a large biogenic secondary organic aerosol event from Eastern Canadian forests, Atmos. Chem. Phys., 10, 2825–2845, doi:10.5194/acp-10-2825-2010, 2010.

Spaulding, R. S., Schade, G. W., Goldstein, A. H., and Charles, M. J.: Characterization of secondary atmospheric photooxidation products: Evidence for biogenic and anthropogenic sources, J. Geophys. Res.-Atmos., 108, 4247, doi:10.1029/2002jd002478, 2003.

Subramanian, R., Kok, G. L., Baumgardner, D., Clarke, A., Shinozuka, Y., Campos, T. L., Heizer, C. G., Stephens, B. B., de Foy, B., Voss, P. B., and Zaveri, R. A.: Black carbon over Mexico: the effect of atmospheric transport on mixing state, mass absorption cross-section, and BC/CO ratios, Atmos. Chem. Phys., 10, 219–237, doi:10.5194/acp-10-219-2010, 2010.

Sullivan, A. P., Peltier, R. E., Brock, C. A., de Gouw, J. A., Holloway, J. S., Warneke, C., Wollny, A. G., and Weber, R. J.: Airborne measurements of carbonaceous aerosol soluble in water over northeastern United States: Method development and an investigation into water-soluble organic carbon sources, J. Geophys. Res.-Atmos., 111, D23S46, doi:10.1029/2006jd007072, 2006.

Sun, Y., Zhang, Q., Macdonald, A. M., Hayden, K., Li, S. M., Liggio, J., Liu, P. S. K., An-

Submicron particles influenced by emissions

A. Setyan et al.

Title Page

Abstract	Introduction
Conclusions	References
Tables	Figures

◄◄	►►
◄	►
Back	Close

Full Screen / Esc

Printer-friendly Version

Interactive Discussion

lauf, K. G., Leaitch, W. R., Steffen, A., Cubison, M., Worsnop, D. R., van Donkelaar, A., and Martin, R. V.: Size-resolved aerosol chemistry on Whistler Mountain, Canada with a high-resolution aerosol mass spectrometer during INTEX-B, Atmos. Chem. Phys., 9, 3095–3111, doi:10.5194/acp-9-3095-2009, 2009.

5 Sun, Y.-L., Zhang, Q., Schwab, J. J., Demerjian, K. L., Chen, W.-N., Bae, M.-S., Hung, H.-M., Hogrefe, O., Frank, B., Rattigan, O. V., and Lin, Y.-C.: Characterization of the sources and processes of organic and inorganic aerosols in New York city with a high-resolution time-of-flight aerosol mass apectrometer, Atmos. Chem. Phys., 11, 1581–1602, doi:10.5194/acp-11-1581-2011, 2011a.

10 Sun, Y. L., Zhang, Q., Zheng, M., Ding, X., Edgerton, E. S., and Wang, X. M.: Characterization and Source Apportionment of Water-Soluble Organic Matter in Atmospheric Fine Particles (PM$_{2.5}$) with High-Resolution Aerosol Mass Spectrometry and GC-MS, Environ. Sci. Technol., 45, 4854–4861, doi:10.1021/es200162h, 2011b.

Ulbrich, I. M., Canagaratna, M. R., Zhang, Q., Worsnop, D. R., and Jimenez, J. L.: Interpreta-
15 tion of organic components from Positive Matrix Factorization of aerosol mass spectrometric data, Atmos. Chem. Phys., 9, 2891–2918, doi:10.5194/acp-9-2891-2009, 2009.

Vaden, T. D., Imre, D., Beranek, J., Shrivastava, M., and Zelenyuk, A.: Evaporation kinetics and phase of laboratory and ambient secondary organic aerosol, Proc. Natl. Acad. Sci. USA, 108, 2190–2195, 2011.

20 Volkamer, R., Jimenez, J. L., San Martini, F., Dzepina, K., Zhang, Q., Salcedo, D., Molina, L. T., Worsnop, D. R., and Molina, M. J.: Secondary organic aerosol formation from anthropogenic air pollution: Rapid and higher than expected, Geophys. Res. Lett., 33, L17811, doi:10.1029/2006gl026899, 2006.

Watson, J. G.: Visibility: Science and regulation, J. Air Waste Manage. Assoc., 52, 628–713,
25 2002.

Weber, R. J., Sullivan, A. P., Peltier, R. E., Russell, A., Yan, B., Zheng, M., de Gouw, J., Warneke, C., Brock, C., Holloway, J. S., Atlas, E. L., and Edgerton, E.: A study of secondary organic aerosol formation in the anthropogenic-influenced southeastern United States, J. Geophys. Res.-Atmos., 112, D13302, doi:10.1029/2007jd008408, 2007.

30 Wiedensohler, A.: An approximation of the bipolar charge distribution for particles in the submicron size range, J. Aerosol. Sci., 19, 387–389, 1988.

Wiedensohler, A., Birmili, W., Nowak, A., Sonntag, A., Weinhold, K., Merkel, M., Wehner, B., Tuch, T., Pfeifer, S., Fiebig, M., Fjäraa, A. M., Asmi, E., Sellegri, K., Depuy, R., Venzac, H.,

Submicron particles influenced by emissions

A. Setyan et al.

Title Page

Abstract	Introduction
Conclusions	References
Tables	Figures

|◄ | ►|

◄ | ►

Back | Close

Full Screen / Esc

Printer-friendly Version

Interactive Discussion

Villani, P., Laj, P., Aalto, P., Ogren, J. A., Swietlicki, E., Roldin, P., Williams, P., Quincey, P., Hüglin, C., Fierz-Schmidhauser, R., Gysel, M., Weingartner, E., Riccobono, F., Santos, S., Grüning, C., Faloon, K., Beddows, D., Harrison, R. M., Monahan, C., Jennings, S. G., O'Dowd, C. D., Marinoni, A., Horn, H.-G., Keck, L., Jiang, J., Scheckman, J., McMurry, P. H., Deng, Z., Zhao, C. S., Moerman, M., Henzing, B., and de Leeuw, G.: Particle mobility size spectrometers: harmonization of technical standards and data structure to facilitate high quality long-term observations of atmospheric particle number size distributions, Atmos. Meas. Tech. Discuss., 3, 5521–5587, doi:10.5194/amtd-3-5521-2010, 2010.

Winklmayr, W., Reischl, G. P., Lindner, A. O., and Berner, A.: A new electromobility spectrometer for the measurement of aerosol size distributions in the size range from 1 to 1000 nm, J. Aerosol. Sci., 22, 289–296, 1991.

Worton, D. R., Goldstein, A. H., Farmer, D. K., Docherty, K. S., Jimenez, J. L., Gilman, J. B., Kuster, W. C., de Gouw, J., Williams, B. J., Kreisberg, N. M., Hering, S. V., Bench, G., McKay, M., Kristensen, K., Glasius, M., Surratt, J. D., and Seinfeld, J. H.: Origins and composition of fine atmospheric carbonaceous aerosol in the Sierra Nevada Mountains, California, Atmos. Chem. Phys., 11, 10219–10241, doi:10.5194/acp-11-10219-2011, 2011.

Zaveri, R. A., Easter, R. C., Fast, J. D., and Peters, L. K.: Model for Simulating Aerosol Interactions and Chemistry (MOSAIC), J. Geophys. Res.-Atmos., 113, doi:10.1029/2007jd008782, 2008.

Zaveri, R. A., Shaw, W. J., Cziczo, D. J., Schmid, B., Ferrare, R. A., Alexander, M. L., Alexandrov, M., Alvarez, R. J., Arnott, W. P., Atkinson, D. B., Baidar, S., Banta, R. M., Barnard, J. C., Beranek, J., Berg, L. K., Brechtel, F., Brewer, W. A., Cahill, J. F., Cairns, B., Cappa, C. D., Chand, D., China, S., Comstock, J. M., Dubey, M. K., Easter, R. C., Erickson, M. H., Fast, J. D., Floerchinger, C., Flowers, B. A., Fortner, E., Gaffney, J. S., Gilles, M. K., Gorkowski, K., Gustafson, W. I., Gyawali, M., Hair, J., Hardesty, R. M., Harworth, J. W., Herndon, S., Hiranuma, N., Hostetler, C., Hubbe, J. M., Jayne, J. T., Jeong, H., Jobson, B. T., Kassianov, E. I., Kleinman, L. I., Kluzek, C., Knighton, B., Kolesar, K. R., Kuang, C., Kubátová, A., Langford, A. O., Laskin, A., Laulainen, N., Marchbanks, R. D., Mazzoleni, C., Mei, F., Moffet, R. C., Nelson, D., Obland, M. D., Oetjen, H., Onasch, T. B., Ortega, I., Ottaviani, M., Pekour, M., Prather, K. A., Radney, J. G., Rogers, R. R., Sandberg, S. P., Sedlacek, A., Senff, C. J., Senum, G., Setyan, A., Shilling, J. E., Shrivastava, M., Song, C., Springston, S. R., Subramanian, R., Suski, K., Tomlinson, J., Volkamer, R., Wallace, H. W., Wang, J., Weickmann, A. M., Worsnop, D. R., Yu, X.-Y., Zelenyuk, A., and

Submicron particles influenced by emissions

A. Setyan et al.

Title Page

Abstract	Introduction
Conclusions	References
Tables	Figures

◀◀　　　▶▶

◀　　　▶

Back　　　Close

Full Screen / Esc

Printer-friendly Version

Interactive Discussion

Zhang, Q.: Overview of the 2010 Carbonaceous Aerosols and Radiative Effects Study (CARES), Atmos. Chem. Phys. Discuss., 12, 1299–1400, doi:10.5194/acpd-12-1299-2012, 2012.

Zhang, Q., Stanier, C. O., Canagaratna, M. R., Jayne, J. T., Worsnop, D. R., Pandis, S. N., and Jimenez, J. L.: Insights into the chemistry of new particle formation and growth events in Pittsburgh based on aerosol mass spectrometry, Environ. Sci. Technol., 38, 4797–4809, doi:10.1021/es035417u, 2004.

Zhang, Q., Alfarra, M. R., Worsnop, D. R., Allan, J. D., Coe, H., Canagaratna, M. R., and Jimenez, J. L.: Deconvolution and quantification of hydrocarbon-like and oxygenated organic aerosols based on aerosol mass spectrometry, Environ. Sci. Technol., 39, 4938–4952, doi:10.1021/es048568l, 2005a.

Zhang, Q., Canagaratna, M. R., Jayne, J. T., Worsnop, D. R., and Jimenez, J. L.: Time- and size-resolved chemical composition of submicron particles in Pittsburgh: Implications for aerosol sources and processes, J. Geophys. Res.-Atmos., 110, D07S09, doi:10.1029/2004jd004649, 2005b.

Zhang, Q., Worsnop, D. R., Canagaratna, M. R., and Jimenez, J. L.: Hydrocarbon-like and oxygenated organic aerosols in Pittsburgh: insights into sources and processes of organic aerosols, Atmos. Chem. Phys., 5, 3289–3311, doi:10.5194/acp-5-3289-2005, 2005c.

Zhang, Q., Jimenez, J. L., Canagaratna, M. R., Allan, J. D., Coe, H., Ulbrich, I., Alfarra, M. R., Takami, A., Middlebrook, A. M., Sun, Y. L., Dzepina, K., Dunlea, E., Docherty, K., DeCarlo, P. F., Salcedo, D., Onasch, T., Jayne, J. T., Miyoshi, T., Shimono, A., Hatakeyama, S., Takegawa, N., Kondo, Y., Schneider, J., Drewnick, F., Borrmann, S., Weimer, S., Demerjian, K., Williams, P., Bower, K., Bahreini, R., Cottrell, L., Griffin, R. J., Rautiainen, J., Sun, J. Y., Zhang, Y. M., and Worsnop, D. R.: Ubiquity and dominance of oxygenated species in organic aerosols in anthropogenically-influenced Northern Hemisphere midlatitudes, Geophys. Res. Lett., 34, L13801, doi:10.1029/2007gl029979, 2007a.

Zhang, Q., Jimenez, J. L., Worsnop, D. R., and Canagaratna, M.: A case study of urban particle acidity and its influence on secondary organic aerosol, Environ. Sci. Technol., 41, 2007b.

Zhang, Q., Jimenez, J., Canagaratna, M., Ulbrich, I., Ng, N., Worsnop, D., and Sun, Y.: Understanding atmospheric organic aerosols via factor analysis of aerosol mass spectrometry: a review, Analyt. Bioanalyt. Chem., 401, 3045–3067, doi:10.1007/s00216-011-5355-y, 2011.

Submicron particles influenced by emissions

A. Setyan et al.

Title Page

Abstract | Introduction

Conclusions | References
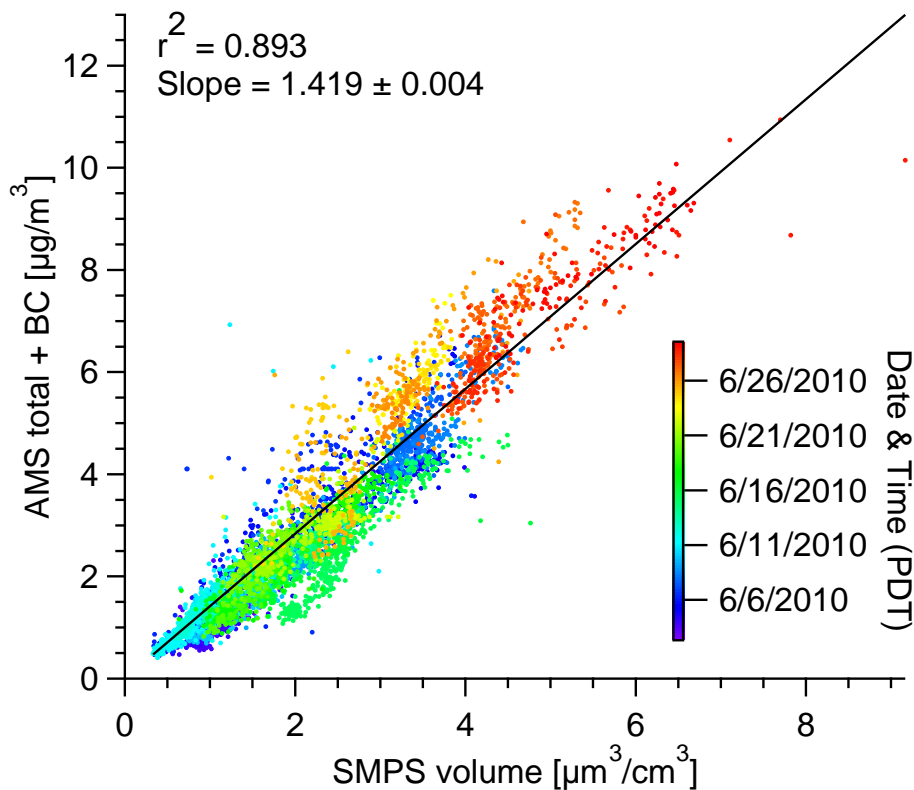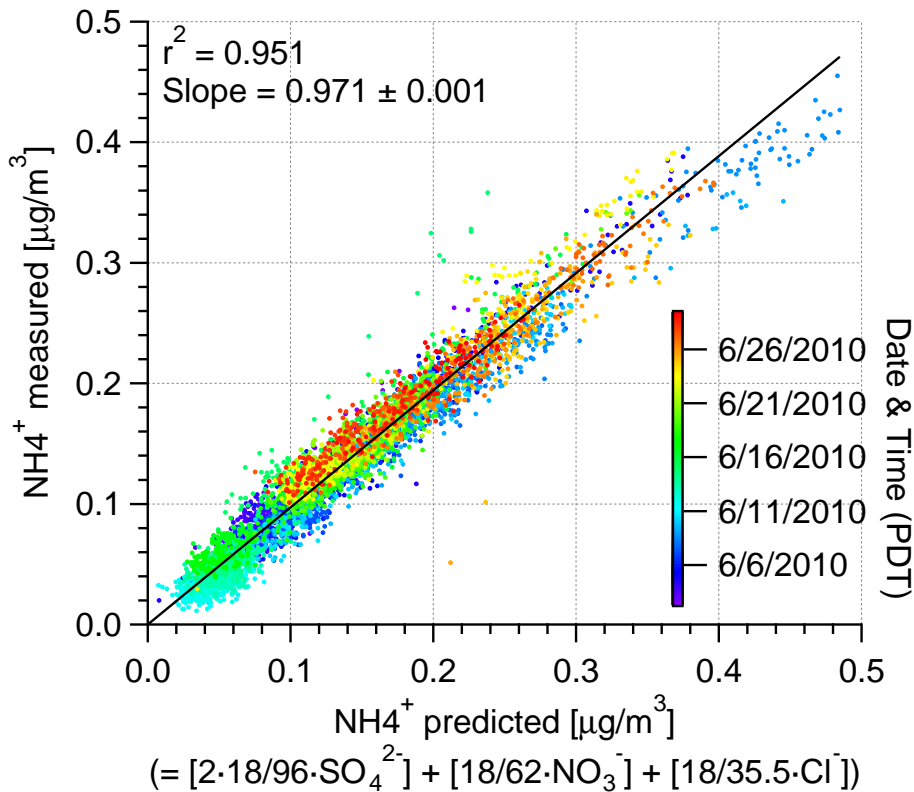
Tables | Figures

◄ | ►

◄ | ►

Back | Close

Full Screen / Esc

Printer-friendly Version

Interactive Discussion

Table 1. Summary of the average concentrations and % of total PM$_1$ or VOCs during the entire study and in the three air masses as marked on Fig. 2.

	Entire study		T0 → T1 transport		Northwesterly wind		Other periods	
	(μg m^{-3})	(% of PM$_1$)	(μg m^{-3})	(% of PM$_1$)	(μg m^{-3})	(% of PM$_1$)	(μg m^{-3})	(% of PM$_1$)
Organics	2.4	80.4	3.1	80	1.4	79	2.6	81
MO-OOA	0.97	40[a]	1.1	36[a]	0.63	44[a]	1.1	42[a]
LO-OOA	1.2	51[a]	1.8	57[a]	0.61	43[a]	1.3	50[a]
HOA	0.22	9.0[a]	0.22	7.2[a]	0.19	13[a]	0.23	8.6[a]
Sulfate	0.30	9.9	0.39	10	0.18	10	0.31	9.6
Nitrate	0.11	3.6	0.13	3.5	0.070	4.0	0.12	3.5
Ammonium	0.13	4.5	0.17	4.4	0.091	5.2	0.14	4.3
Chloride	0.002	0.1	< DL[b]	0.1	<DL[b]	0.0	< DL[b]	0.1
Black Carbon	0.07	1.6	0.054	1.4	0.032	1.8	0.053	1.6
Total PM$_1$[c]	3.0		3.9		1.8		3.3	
	(ppb)	(% of VOC)	(ppb)	(% of VOC)	(ppb)	(% of VOC)	(ppb)	(% of VOC)
Photo-oxidation products[d]	7.6	82	8.3	81	5.6	79	7.9	83
Biogenic VOCs[e]	1.5	16	1.7	17	1.3	18	1.4	14
Aromatic VOCs[f]	0.23	2.4	0.19	1.8	0.19	2.7	0.27	2.8
Total VOCs	9.3		10.2		7.1		9.6	

[a] % of total organics
[b] Detection limit
[c] Total PM$_1$ = Org + SO$_4^{2-}$ + NO$_3^-$ + NH$_4^+$ + Ch$^-$ + BC
[d] Photo-oxidation products = acetaldehyde + acetic acid + methacrolein + methyl vinyl ketone + methyl ethyl ketone + formaldehyde + acetone
[e] Biogenic VOCs = isoprene + monoterpenes + 2-methyl-3-buten-2-ol + methyl chavicol
[f] Aromatic VOCs = benzene + C2-benzenes + C3-benzenes + C4-benzenes + toluene
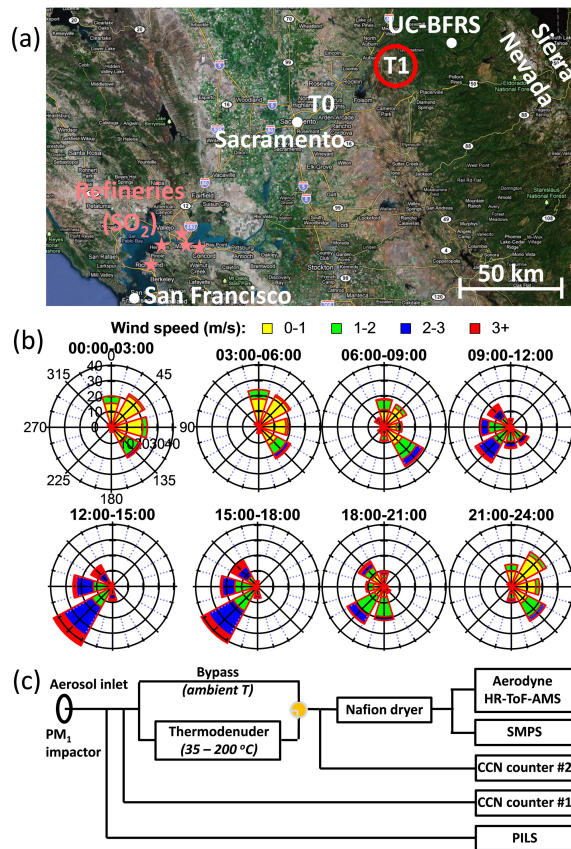
Fig. 1. (a) Map of the Sacramento Valley with the location of the two ground-based sites (T0 and T1) and that of the University of California-Blodgett Forest Research Station (UC-BFRS, site of the BEARPEX 2007 and 2009 studies). **(b)** Wind rose plots for every 3-h period at the T1 site (height: 3 m), colored by wind speed. Radial scales correspond to the frequency, and are kept the same in each wind rose. **(c)** Schematic drawing of the instrumental setup.

Title Page

Abstract | Introduction

Conclusions | References

Tables | Figures

◄ | ►I

◄ | ►

Back | Close

Full Screen / Esc

Printer-friendly Version

Interactive Discussion
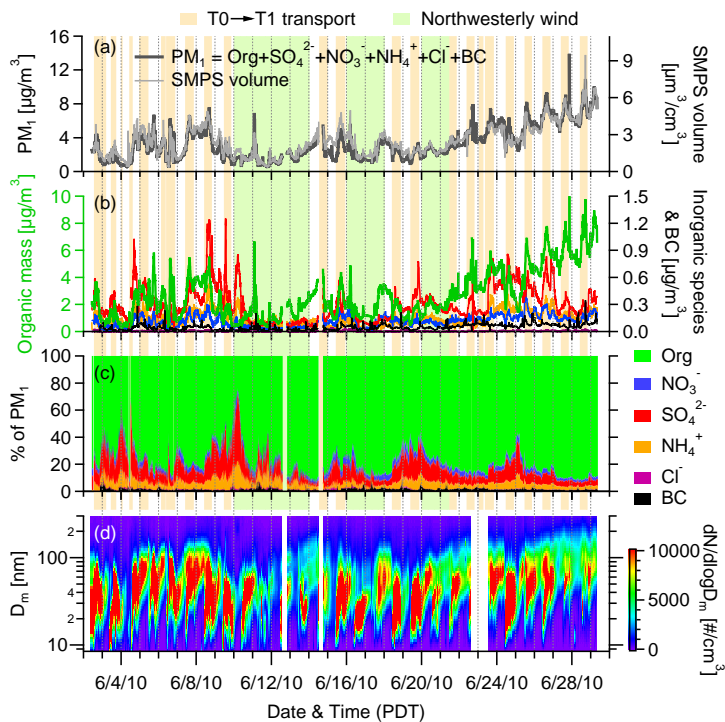
Fig. 2. Time series of **(a)** AMS total mass + BC and SMPS volume concentrations, **(b)** concentrations of organics (left y-axis), sulfate, nitrate, ammonium, chloride, and BC (right y-axis), **(c)** percentage contribution of the species to the total PM_1 mass, and **(d)** particle number size distribution by the SMPS. BC data is not available before 6 March 2010, so PM_1 concentrations before this date correspond to the sum of NR-PM_1 (AMS species). Shaded regions indicate 23 periods of urban plumes transported from T0 to T1 (orange) and 3 periods subjected to influences from northwesterly wind (green). The remaining periods correspond mainly to downslope flows from the Sierra Nevada to the foothills.

Title Page

Abstract | Introduction

Conclusions | References

Tables | Figures

◄ | ►

◄ | ►

Back | Close

Full Screen / Esc

Printer-friendly Version

Interactive Discussion

Fig. 3. Scatterplot of AMS total + BC mass vs. SMPS volume in the size range 25–714 nm (D_{m}), colored by time.

Fig. 4. Scatterplot of NH_4^+ measured vs. NH_4^+ predicted, colored by time.

Full Screen / Esc

Printer-friendly Version

Interactive Discussion
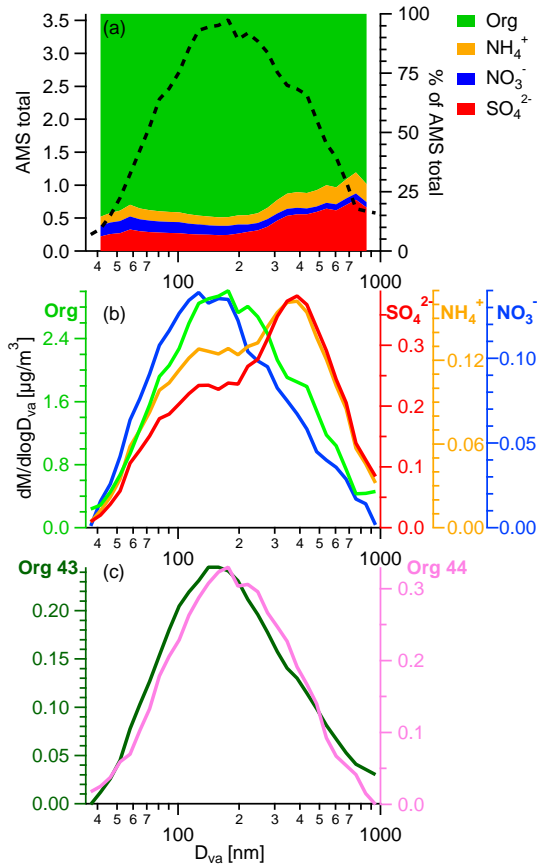
Fig. 5. (a) Average size distributions of the AMS total mass and percentage contribution of aerosol species to total mass, **(b)** average size distributions of aerosol species, and **(c)** average size distributions of organic aerosol signals at *m/z* 43 and *m/z* 44.
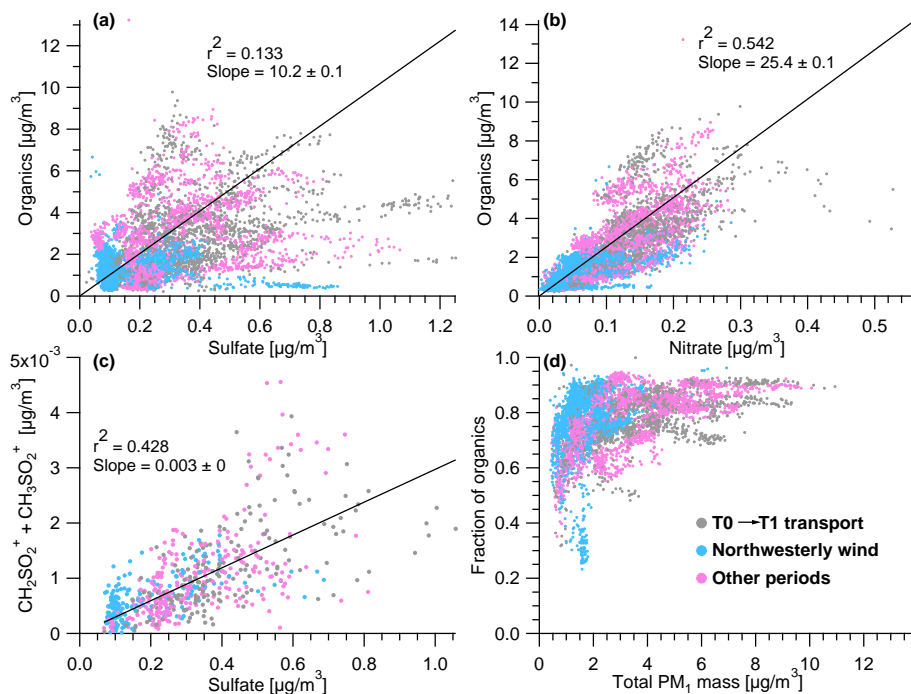
Fig. 6. Scatterplots of **(a)** organics vs. sulfate, **(b)** organicsvs. nitrate, **(c)** sum of the main MSA ions vs. sulfate (1-h averaged data), and **(d)** fraction of organicsvs. PM_1 mass. All the scatterplots are colored by air mass types.
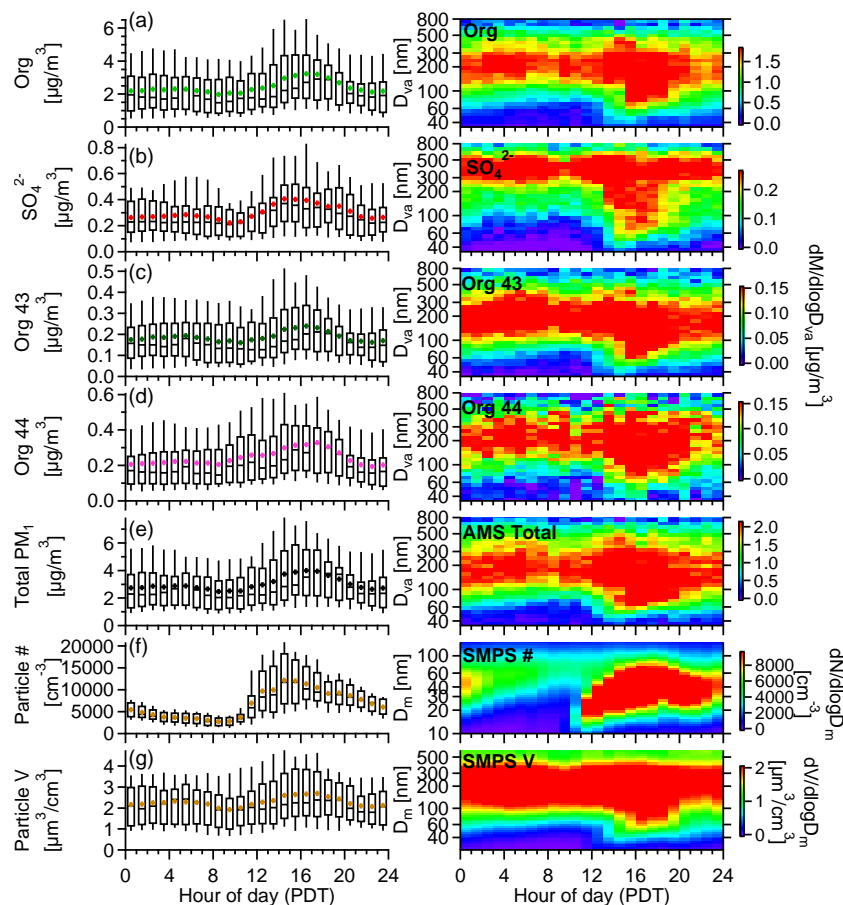
Fig. 7. Diurnal patterns (left panel) and diurnal size distributions (right panel) of **(a)** organics, **(b)** sulfate, **(c)** Org 43, **(d)** Org 44, **(e)** AMS total mass, **(f)** particle number, and **(g)** volume concentrations.
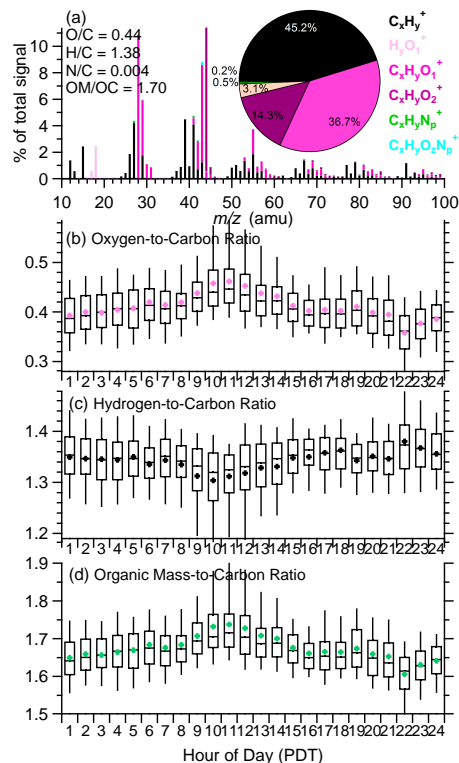
Fig. 8. (a) Average high resolution mass spectrum of organics colored by ion category, along with a pie chart with the contribution of each ion category to the total signal. Diurnal patterns of **(b)** O/C ratio, **(c)** H/C ratio, and **(d)** OM/OC ratio of organics. The $C_xH_yS_nO_z^+$ family is not shown in the pie chart due to its very small contribution (average = 0.09 %).

Title Page

Abstract | Introduction

Conclusions | References

Tables | Figures

◀ | ▶|

◀ | ▶

Back | Close

Full Screen / Esc

Printer-friendly Version

Interactive Discussion
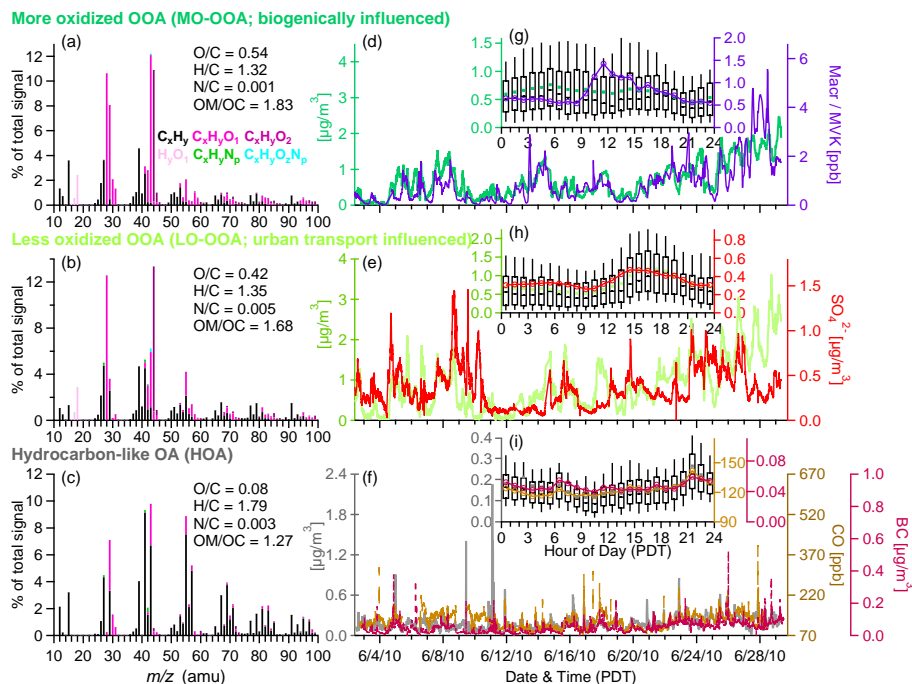
Fig. 9. High-resolution mass spectra (colored by ion category) and elemental ratios of the OA factors **(a–c)**, along with their time series **(d–f)** and diurnal patterns **(g–i)**, and those of tracer compounds.

Fig. 10. Average contribution of ion categories to the total signal of the three OA factors **(a)**, and average contribution of OA factors to the three main ion categories **(b)**.
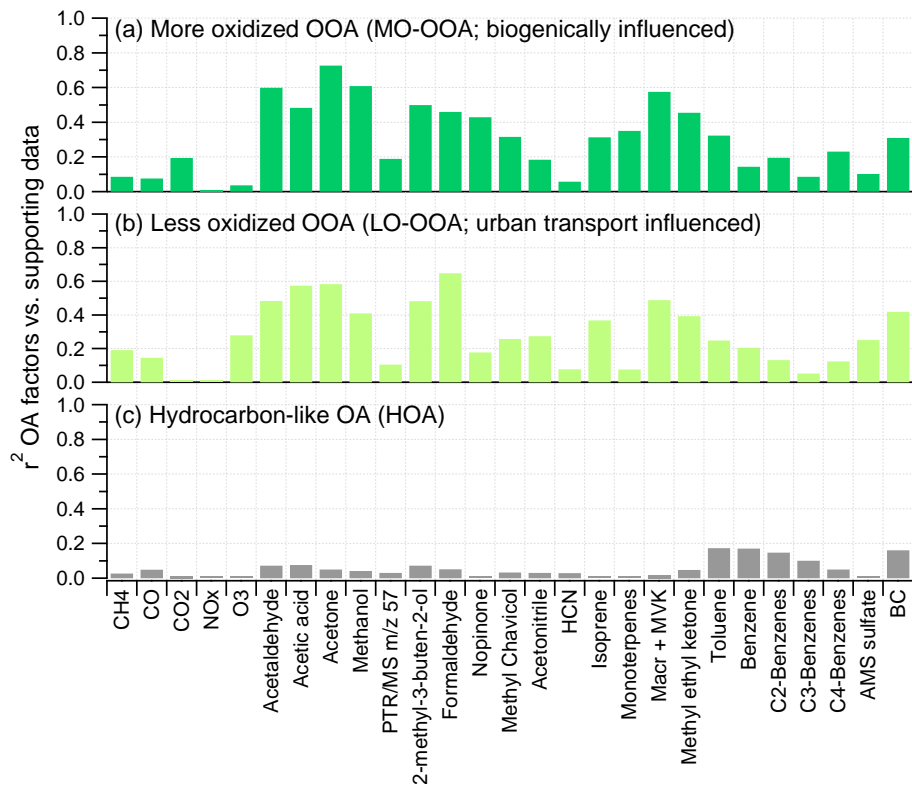
Fig. 11. List of correlation coefficients (r^2) between OA factors and trace gases, VOCs, AMS sulfate and BC. Signal at *m/z* 57 recorded by the PTR/MS corresponds mainly to butanol, with contribution of other compounds.
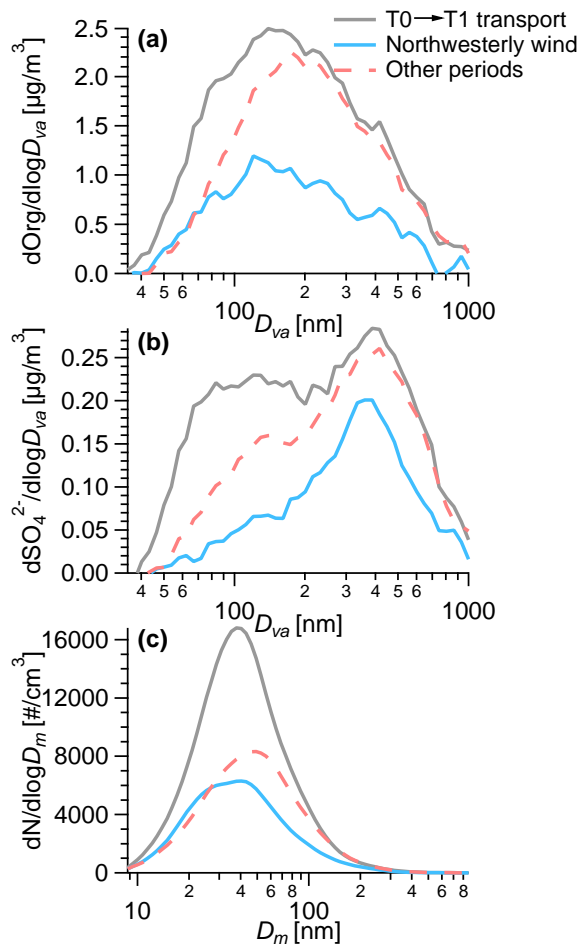
Title Page

Abstract | Introduction

Conclusions | References

Tables | Figures

◄◄ | ►►

◄ | ►

Back | Close

Full Screen / Esc

Printer-friendly Version

Interactive Discussion
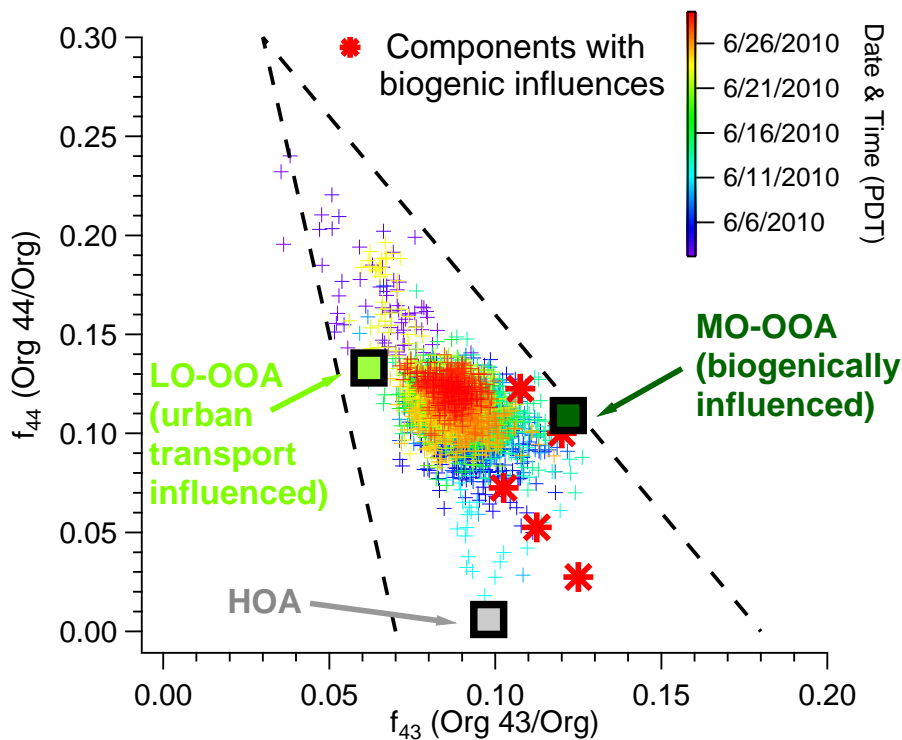
Fig. 12. Triangle plot (f_{44} vs. f_{43}) with ambient data (colored by time) and OA factors. The triangle region was determined by Ng et al. (2010) and corresponds to region where ambient OOA factors from different datasets fall. Red star points correspond to OOA factors previously published and reporting biogenic influences (Allan et al., 2006; Cottrell et al., 2008; Sun et al., 2009; Raatikainen et al., 2010; Slowik et al., 2010).

Title Page

Abstract | Introduction

Conclusions | References

Tables | Figures

|◄ | ►|

◄ | ►

Back | Close

Full Screen / Esc

Printer-friendly Version

Interactive Discussion

Fig. 13. Comparison of the average size distributions of **(a)** organics, **(b)** sulfate and **(c)** particle number concentration between the three air mass categories as marked on Fig. 2.
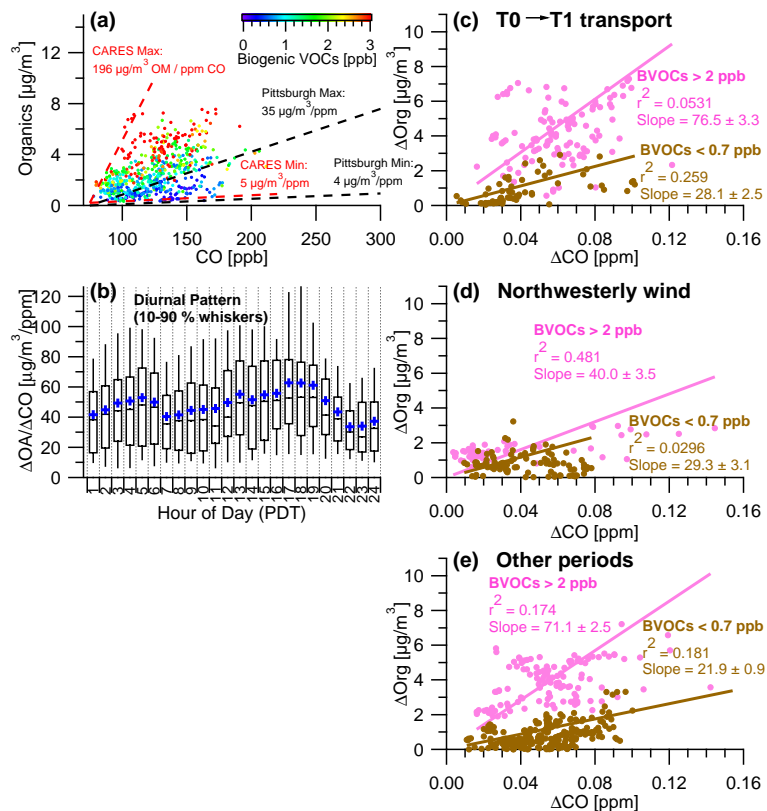
Fig. 14. **(a)** Scatterplot of organics vs. CO, colored by the sum of biogenic VOCs (= isoprene + monoterpenes + 2-methyl-3-buten-2-ol [MBO] + methyl chavicol). **(b)** Diurnal pattern of ΔOA/ΔCO. Scatterplot of ΔOA/ΔCO during three air mass types as marked on Fig. 2: **(c)** T0 to T1 transport, **(d)** northwesterly wind and **(e)** other periods. In **(c–e)**, the data points are classified into periods of high (>2 ppb) or low (<0.7 ppb) mixing ratios of biogenic VOCs.